A Study of the Spring Phytoplankton Blooms

in Cyclonic and Anticyclonic Mesoscale Eddies

（低気圧性・高気圧性中規模渦における

植物プランクトン春季大増殖に関する研究）

MAÚRE, Elígio de Raús

（マウレ　エリジオ　デ　ラウシ）

A dissertation for the degree of Doctor of Environmental Sciences

Department of Earth and Environmental Sciences,

Graduate School of Environmental Studies, Nagoya University

（名古屋大学大学院環境学研究科地球環境科学専攻学位論文　博士（環境学））

2018

Abstract

Phytoplankton productivity fuels life in the oceans through energy transfer to higher trophic levels and plays a major role in biogeochemical cycles and climate. Moreover, in temperate seas where seasonality of phytoplankton production occurs, the amount of energy transferred to higher trophic levels is largely influenced by the timing and magnitude of phytoplankton blooms. Phytoplankton production is regulated by nutrient and light availability for photosynthesis. Mesoscale eddy is one of the physical features with a major role in the regulation of primary production. Through modulation of mixed layer depth, they are potentially capable of simultaneously impacting the light field and nutrient availability. Thus, an understanding of their integrated impacts on biological activity improves our understanding of physical-biological interactions and their consequent role on marine ecosystem dynamics and biological carbon pump in the ocean under climate change.

Objective of this study is to investigate the influence of mesoscale eddies on the dynamics of spring phytoplankton blooms in temperate regions. The Japan Sea is used as a case study given that it is a temperate sea where large seasonal phytoplankton variability and strong eddy activity occur. Therefore, it provides a good opportunity to investigate the mechanism by which mesoscale eddies impact the seasonal cycle of phytoplankton productivity, in particular, the initiation of the spring blooms.

The first part (Chapter 2) of this work employs chlorophyll a (CHL) concentration and sea level anomaly (SLA) data from satellite measurements in combination with *in situ* profiles of temperature and salinity to construct composites within eddies in order to investigate their impact on the initiation of the spring phytoplankton blooms. SLA and *in situ* data were used to obtain the information of mesoscale eddy field and to estimate the mixed-layer depth in the interior of eddies, respectively, around the Yamato Basin (133-139º E and

35-39.5º N) in the Japan Sea. CHL time series were analysed along with obtained mixed-layer depth to evaluate the timing of spring phytoplankton bloom initiation associated with mesoscale AEs and CEs in the Japan Sea, for the period 2002-2011. The results showed significant differences between AEs and CEs in the timing of the spring phytoplankton blooms. Blooms were initiated earlier in CEs characterized by shallow mixed-layer depths (<100 m). The early blooming preceded the end of winter cooling (i.e., while net heat flux (Q0) is still negative) and is associated with the increased average light within the shallow mixed-layer depth. Conversely, blooms appeared in the AEs despite deeper mixed-layer depth (>100 m) but close to the commencement of positive Q0. This suggests that the relaxation of turbulent mixing is crucial for the bloom initiation in AEs.

Based on the above findings, in the second part (Chapter 3) of this work, a four-compartment model that simulates the interactions of nutrient-phytoplankton-zooplankton-detritus (NPZD) coupled to a one-dimensional (1D) Mellor-Yamada based turbulence closure model is used to study the mechanism of spring bloom initiation associated with eddies. This lower trophic ecosystem model is used to obtain a detailed picture of phytoplankton dynamics in eddies and to verify the results obtained in Chapter 2. Unlike satellite data that may be missing under cloud coverage and *in situ* measurements with paucity of data, the model output has the advantage of providing high vertical and temporal resolution needed to fully investigate the variations in phytoplankton prior and during the spring bloom initiation. The experiment is performed using realistic forcing obtained and averaged over the eddy tracks for eddies identified and tracked in the study region. The results from the turbulence model showed that weakening of turbulent mixing is crucial for blooms to be triggered in AEs with deep mixed-layer. However, in CEs with shallow mixed-layers, the onset of spring blooms developed in the presence of strong turbulence, i. e., during strong net cooling. In this case, increasing surface irradiance improves the light condition within the shallow mixed-

layer and triggers the spring blooms. Moreover, the biological model also showed that in AEs, a gradual phytoplankton accumulation phase begins in winter when zooplankton grazing decreases considerably. However, the initiation of the spring blooms followed in spring with the exponential growth. In CEs, the winter phytoplankton accumulation was faster, and this was also a reason of the faster phytoplankton peak in spring.

This study provides the first insight into the effects of mesoscale eddies present in the global ocean on the timing of spring bloom initiation. Distinct mechanisms showed by this study in AEs and CEs regulating the initiation of spring phytoplankton blooms are general and may apply to other regions in the global ocean where eddies proliferate. Therefore, role of mesoscale eddies on bloom variability should be incorporated into a general framework of seasonal cycle of phytoplankton bloom. Finally, the difference in initiation timing of AEs and CEs is expected to have different impacts on recruitment success of different fish species in many parts of the global ocean.

要旨

植物プランクトンの生産は、高次生産レベルへのエネルギーの転換を通して海洋の生命を支え、生物地球化学循環や気候調整に重要な役割を果たす。植物プランクトンの生産の季節変動が起こる温帯域では、高次生産レベルへのエネルギーの転換が植物プランクトンの季節的な大増殖のタイミングや大きさに強く影響を受ける。植物プランクトンの生産は、光合成への栄養塩と光の供給量で制御されている。中規模渦は基礎生産の制御に主要な役割を果たす物理過程の一つである。これらは混合層の調整を通して、光分布と栄養塩の供給量に同時に影響を与える可能性がある。従って、中規模渦の生物活動への統合的な影響を理解することは、物理－生物相互作用とその気候変動下での海洋生態系動態および生物的炭素ポンプへの役割についての理解を深める。

この研究の目的は、温帯海域での春季の植物プランクトン大増殖動態への中規模渦の影響を調べることである。植物プランクトンの大きな季節変動と、活発な渦活動の知られる温帯海域である日本海を事例研究として使った。この研究は、中規模渦が植物プランクトンによる生産の季節変動、特に春季大増殖の開始に影響を与える機構を研究する機会を与える。

まず最初に第２章では、植物プランクトンの春季大増殖の開始への影響を調べるために、衛星で測定したクロロフィル a（CHL）濃度と海表面レベル偏差データ（SLA）を、現場渦中の水温・塩分の鉛直分布と組み合わせて解析した。日本海の大和海盆（133-139º E, 35-39.5º N）で、SLA と現場データから中規模渦の情報を得て、渦内部の混合層深度を推定した。また 2002 年から 2011 年の日本海の低気圧性渦と高気圧性渦それぞれの内部における植物プランクトンの春季大増殖の開

始のタイミングを評価するために、CHL の時系列を混合層深度とともに解析した。この結果、高気圧性渦と低気圧性渦では、春季大増殖の時期が有意に異なることが示された。混合層が浅い（<100m）低気圧性渦では、大増殖は早く始まった。この早い大増殖は、冬の冷却が終わる前に（つまり、熱フラックス（Q_0）がまだ正の時に)、浅い混合層の中での平均光強度が増加する時で始まった。反対に高気圧性渦では大増殖の開始が遅く、混合層が深い（>100m）にも関わらず、Q_0 が正になった時に起こった。このことは、混合層内で乱流混合が弱まることが、高気圧性渦内での大増殖の開始に重要であることを示している。

第３章では、第２章で述べた発見に基づいて、栄養塩－植物プランクトン－動物プランクトン－デトリタス（NPZD）の相互作用を鉛直一次元 Mellor-Yamada 乱流モデルと組み合わせた生態系モデルでシミュレーションし、渦による春季大増殖の開始メカニズムを研究した。この低次生産生態系モデルを使って、渦内での植物プランクトン動態の詳細を再現し、第２章で得られた結果を検証した。雲によってデータが欠損する衛星やデータの少ない現場観測と異なり、モデル出力は春季ブルーム開始から終了までの植物プランクトンの変化を完全に研究するのに必要な、鉛直的・時間的に高い解像度を持つ。研究海域で認識し追跡した渦での実際の強制力を使用して実験を行った。乱流モデルの結果から、混合層の深い高気圧性渦では、乱流が弱まることが大増殖の開始に重要であることが明らかとなった。しかし、混合層の浅い低気圧性渦では、冬季の強い乱流混合の中で春季大増殖が進んだ。この場合、日射量の増加による、浅い混合層内での光条件の向上が春季大増殖を引き起こす。さらに生態系モデルは、高気圧性渦内では、冬季に動物プランクトンの摂餌が大きく減少することで、徐々に植物プランクトンが蓄積することを示した。しか

し、植物プランクトンのブルームの開始は、春季の指数増殖によった。低気圧性渦では、冬季の植物プランクトンの蓄積速度は速く、これも春季の植物プランクトンの極大が早い理由となった。

この研究は、世界中の海に存在する中規模渦の植物プランクトンの春季大増殖の開始に対する影響を初めて明らかにした。この高気圧性と低気圧性の渦での研究によって明らかとなった、春季大増殖の開始を制御する機構は一般的であり、渦が活発な他の地球規模海域にも当てはめられる可能性がある。従って、地球規模の海での植物プランクトン大増殖の季節周期の一般的な概念に中規模渦の役割を組み込む必要がある。最後に、世界中の海の多くの場所で、この開始時期の違いは異なる種類の魚のリクルートメントの成功に異なる影響を与えることが予想される。

Contents

List of Tables

List of Figures

Abbreviations

AEs	Anticyclonic eddies
CEs	Cyclonic eddies
CHL	Chlorophyll-*a*
DET	Detritus
DIN	Dissolved inorganic nitrogen
I_{ML}	Mixed-layer averaged light
MERIS	Medium-Resolution Imaging Spectrometer
MLD	Mixed-layer depth
MODIS	Moderate Resolution Imaging Spectroradiometer
NPZD	Nutrient-phytoplankton-zooplankton-detritus
PHY	Phytoplankton
SeaWiFS	Sea-Viewing Wide Field-of-View Sensor
SLA	Sea level anomaly
TKE	Turbulent kinetic energy
TLD	Turbulent layer depth
Z_{eu}	Euphotic layer depth
ZOO	Zooplankton

Symbols

C	Carbon
c_p	Specific heat of water (J $\mathrm{kg^{-1}\ ^{\circ}C^{-1}}$)
f	Coriolis parameter (rad s^{-1})
g	Acceleration due to gravity (m s^{-2})
$g_{\max}$	Zooplankton maximum grazing rate at 0°C (s^{-1})
I_{opt}	Optimum light intensity (W m^{-2})
I_z	Depth profile of light in the water (W m^{-2})
I_0	Surface light intensity (E m^{-2} d^{-1} (W m^{-2} in the physical model))
k_D	Light attenuation by detritus ($\mathrm{m^2 mmolN^{-1}}$)
k_N	Half saturation constant for DIN ($\mathrm{mmolN\ m^{-3}}$)
k_P	Self-shading coefficient of phytoplankton ($\mathrm{m^2 mmolN^{-1}}$)
k_R	Temperature coefficient for respiration ($\mathrm{^{\circ}C^{-1}}$)
k_T	Temperature coefficient ($\mathrm{^{\circ}C^{-1}}$)
k_W	Light dissipation coefficient of seawater (m^{-1})
L_I	Light limitation function
L_N	Nutrient limitation function
M_P	Phytoplankton mortality rate at 0°C ($\mathrm{m^3 (mmolN\ s)^{-1}}$)
M_Z	Zooplankton mortality rate at 0°C ($\mathrm{m^3 (mmolN\ s)^{-1}}$)
N	Nitrogen
Q_0	Surface net heat flux (W m^{-2})
r	Correlation coefficient
R	Restoration rate (s^{-1})
r_{DN}	Detritus decomposition rate at 0°C (s^{-1})

r_P	Net phytoplankton accumulation rate (s^{-1})
R_P	Phytoplankton respiration rate at 0°C ($℃^{-1}$)
r_{TLD}	Rate of change of mixed–layer depth (s^{-1})
S	Salinity
T	Temperature (℃)
u	Horizontal component of velocity along x-axis (m s^{-1})
U_P	Phytoplankton photosynthetic rate (s^{-1})
v	Horizontal component of velocity along y-axis (m s^{-1})
w_D	Sinking speed of detritus (m s^{-1})
w_P	Sinking speed of phytoplankton (m s^{-1})
α_Z	Zooplankton assimilation efficiency
β_Z	Zooplankton growth efficiency
κ	Eddy diffusivity (m^2 s^{-1})
λ	Ivlev constant ($m^3(mmolN\ s)^{-1}$)
$\mu_{\max}$	Phytoplankton Maximum photosynthetic rate at 0°C (s^{-1})
ν	Eddy viscosity (m^2 s^{-1})
ρ_0	Surface density (kg m^{-3})
σ	Stefan-Boltzmann constant in the physical model ($Wm^{-2}K^{-4}$)
σ	Threshold value for grazing in the biological model ($mmolN\ m^{-3}$)
τ	Wind stress (N m^{-2})

Chapter 1

1. Introduction and Motivation

Mesoscale eddies play an important role in the transport of heat and freshwater as well as in the upper-ocean circulation. Therefore, they contribute on the regulation of global heat budget and climate (e.g., Dong et al. 2014; Zhang et al. 2014). In addition, the distribution of other oceanic tracers, such as nitrogenous nutrients, is also horizontally and vertically perturbed by the presence of mesoscale eddies (McGillicuddy and Robinson 1997; McGillicuddy et al. 1998). Consequently, their influence also extends to marine productivity and biogeochemical processes (Falkowski et al. 1991; McGillicuddy et al. 1999; Sukigara et al. 2014).

One of the first dedicated multidisciplinary studies aimed at investigating different aspects of the physics, chemistry and biology of mesoscale eddy fields came from the Ring Group in the Gulf Stream (Ring Group 1981). These early studies provided a wealth of information concerning the unique features of mesoscale eddies relative to their surrounding and their potential role in marine ecosystem dynamics, from planktonic primary producers to large predators (Wiebe et al. 1976).

Although a full understanding of their impacts remains limited by the paucity of physical, chemical and biological observations within their interiors, the advent of satellite measurements and the recent increase in the global coverage of Argo float network have significantly contributed to improving our understanding of the physical-biological interactions at the mesoscale. Gaube et al. (2014) used satellite measurements to provide one of the first global overview of the different mechanisms by which mesoscale eddies influence the near-surface chlorophyll *a* (CHL) concentration, namely, the horizontal advection of

phytoplankton around the peripheries of eddies, the physical transport of ecosystems entrapped within the cores of eddies, upwelling, downwelling, and eddy-induced changes in stratification. Furthermore, it was shown that this influence varied regionally and that CHL within an eddy could be influenced by one or more of the aforementioned biophysical processes (Gaube et al. 2014; McGillicuddy 2016) although globally, the azimuthal advection of CHL around eddy peripheries was found to be a dominant mechanism (Chelton et al. 2011a; Gaube et al. 2014).

Given that mesoscales eddies bring about changes in stratification and thus influence mixed layer dynamics, detailed understanding of their physics is fundamental to understanding their potential role in regulating phytoplankton seasonality and biogeochemical fluxes. The surface mixed layer is where the transport of heat and freshwater, the exchange of gases between the ocean and the overlying atmosphere takes place (Ferrari and Boccaletti 2004). It plays a fundamental role not only in climate but also in ocean primary production that is also limited to the upper sunlit area of the ocean. Dufois et al., (2016) suggested that vertical mixing resulting from buoyancy loss to the atmosphere have a significant impact on phytoplankton seasonal cycle associated with subtropical gyre mesoscale eddies.

The overarching goal of this study is to examine the influence of mesoscale eddies on the seasonality of phytoplankton productivity in temperate oceans. Satellite and *in situ* measurements within eddies have been examined to gain insights on the impacts of eddies on the seasonal cycle of CHL. Furthermore, to better resolve the temporal variability of primary production in the interior of mesoscale eddies, a nutrient-phytoplankton-zooplankton-detritus (NPZD) model coupled to a 1D mixed-layer turbulence physical model is used to investigate the details of the dynamics of the mixed layer and the evolution of plankton within mesoscale eddies.

1.1. Generation, Identification and Tracking of Mesoscale Eddies

Ocean dynamics is dominated by a spectrum of processes spanning a great variety of space-time scales, from as small-rapid as a few millimetre-second scales such as turbulent motions to as large-long as basin-year scales as ocean circulation (Mann and Lazier 1996). Mesoscale processes, which fall within the spatial and temporal scales of tens to hundreds of kilometres and of days to months, respectively, are among the most energetic of oceanic motions. Mesoscale eddy fields also include a rich cascade of features like meanders and filaments. However, most of the interest is concentrated on the coherent vortices (Chelton et al. 2007, 2011b; Dong et al. 2014) given their unique ability to cause anomalies in regions other than where they are generated.

Mesoscale eddies are circular currents in the ocean and are generated by a number of processes associated with the dynamics of ocean circulation among which baroclinic instability (e.g., conversion of potential energy into kinetic energy or vertically sheared currents) is known to be one of the globally dominant forcing mechanism (e.g., Beckmann et al. 1993; Chelton et al. 2011b). They are found virtually everywhere in the global ocean, but the western boundary currents–the strongest ocean currents–stand out as the regions with the largest amplitude eddies (Chelton et al. 2011b).

Different parts of the global ocean exhibit different eddy generation mechanisms. In the Gulf Stream region, for instance, AEs are formed by the separation, to the north, of the meandering Gulf Stream. These eddies have a typical diameter of 100-200 km (Schink et al. 1981). CEs are generated by the south meandering Gulf Stream. The growing meander becomes unstable and eventually detaches into a separate ring or eddy (Ring Group 1981; McGillicuddy 2016). The Leeuwin Current, in the west coast of Australia, also meanders along the shelf-break and pinch-off AEs. These meanders generating AEs are suggested to be initially associated with CEs (Pearce et al. 1990). An interesting and contrasting feature

between the above two oceanic regions is that in the Gulf Stream AEs entrain open ocean waters during their formation, whereas in the Leeuwin Current AEs entrain shelf water (Schink et al. 1981; Pearce et al. 1990). In the frontal region of the Kuroshio and the Oyashio AEs with diameters of more than 130 km are also known to generate through meandering of the northward protruding Kuroshio (Kitano 1975). Similar to the Gulf Stream the AEs generated in the Kuroshio frontal region also move to cold water region.

The ubiquitous eddies found all over the global ocean cause a characteristic signal at the sea surface, and therefore can be identified on the basis of satellite measurements. Signatures of sea level anomaly (SLA) data provided by AVISO (http://www.aviso.altimetry.fr/), constructed by merging two concurrent altimetry measurements at 0.25º and 7-day spatial and temporal resolution, are routinely used in the identification and tracking of mesoscale eddies.

Automated eddy identification and tracking algorithms have been developed for the identification of eddies in SLA maps (Isern-Fontanet et al. 2003) and in a high resolution data such as numerical model simulations (e.g., Nencioli et al. 2010) for both regional (e.g., Chaigneau et al. 2008) and global (e.g., Chelton et al. 2007, 2011b) studies. These methods identify eddies either based on physical properties of coherent vortices such as the Okubo-Weiss parameter, which provides a measure based on the relative importance of deformation and rotation (e.g., Isern-Fontanet et al. 2003), or on the geometrical properties of the eddy velocity field (Nencioli et al. 2010). In the latter case, eddy centres are identified based on four constraints characterising the spatial distribution of velocity vectors in the presence of eddies namely,

(1) identification, along the latitude, of regions of reversal in sign and increase in magnitude of meridional component of velocity (v) across the eddy centre;

(2) identification, along the longitude, of regions of reversal in sign and increase in magnitude of zonal component of velocity (u) across the eddy centre. The sense of rotation has to be the same with that of v;

(3) identification of regions of local minimum in velocity magnitude at the eddy centre; and

(4) around the eddy centre, the directions of the velocity vectors have to change with a constant sense of rotation (Nencioli et al. 2010). This sense of rotation defines whether the eddy is clockwise rotating (anticyclonic in the northern hemisphere, Figure 1.1) or anticlockwise rotating (cyclonic in the northern hemisphere) eddy. The zonal and meridional components of velocity were computed based on geostrophic approximation as $u = -\frac{g}{f}\frac{\partial SLA}{\partial y}$ and $v = \frac{g}{f}\frac{\partial SLA}{\partial x}$, where g is the gravitational acceleration and f is the Coriolis parameter (Chelton et al. 2007).

In this study, the latter method was adopted given its efficiency in detecting eddies. As compared to the Okubo-Weiss and other methods, the geometric method performs better (Nencioli et al. 2010). Nevertheless, the shortcoming of the geometrical based approach is that eddies are assumed to be circular and those with largely elliptical shapes can at times go undetected. Chelton et al. (2011b) identified eddies entirely based on SLA. In their approach, eddies are identied based on closed contours of SLA. The amplitude of an eddy is defined as the magnitude of the diference betweed the SLA at the eddy perimeter and the extremum SLA within the eddy interior. Eddy interior is the area enclosed by the closed SLA defining the eddy. A speed-based shape of an eddy was defined as the area equal to that within the closed contour of SLA that has the maximum average geostrophic speed (Chelton et al. 2011b). The rotational speed of an eddy corresponds to the average geostrophic speed of the contour defining the speed-based shape. Eddy tracks were constructed according to the procedure detailed in Nencioli et al. (2010).

1.2. Phytoplankton Phenology

Phenology—as defined by the oxford dictionaries—refers to the study of cyclic and seasonal natural phenomena, especially in relation to climate and plant and animal life. In this study, the focus is on the phenology of phytoplankton. Phytoplankton—also known as microalgae—are microscopic plants in the ocean. Similar to plants in land, phytoplankton also contain chlorophyll and need solar energy and inorganic nutrients such as nitrates, phosphates, and silicates to produce proteins, fats, and carbohydrates to support their life and growth. Most phytoplankton, in contrast to land plants, are buoyant and float in the upper iluminated part of the ocean.

The spring bloom—a rapid increase in phytoplankton biomass—occurs in spring when the nutrient concentrations are high and the solar radiation is increasing. The spring bloom has important roles for higher trophic levels and carbon export (Omand et al. 2015; Kodama et al. 2018). The role of physical factors for the spring bloom event have been central in the discussion of the mechanism initiating a bloom (Riley 1942, Sverdrup 1953). The first quantitative description of phytoplankton phenology was provided by Sverdrup (1953) and in his description of the conditions leading to initiate a bloom, light exposure of phytoplankton and turbulent mixing that circulates phytoplankton over deep layers played a crucial role. Based on the Sverdrup model, there is a depth called the critical depth where integrated photosynthic production of phytoplankton just matches the integrated destruction due to respiration. In winter months, phytoplankton growth is light-limited due to combined effetcs of deep mixing and low light condition. For a bloom to occur, the depth to which phytoplankton is being circulated or mixed should be smaller that the critical depth. In spring, increase in solar radiation warms the upper part of the ocean and near-surface stratification is developed. The mixed layer then decreases below the critical depth and favourable light conditions for net phytoplankton growth are created.

In this study, in order to investigate the influence of mesoscale eddies on the spring bloom initiation in temperate ocean, the Japan Sea—a semi-enclosed marginal sea in the northwestern Pacific—was selected as a case study region. Under the influence of monsoonal wind, the Japan Sea is a relatively small and very dynamic sea with special characteristics typical of the global ocean. Often called "a miniature ocean", it has circulation and hydrographical characteristics that resemble that of the global ocean. For instance, a system of deep convection, a western boundary current, a subpolar front, and mesoscales eddies are features that are common to the global ocean found in the Japan Sea (Ichiye 1984; Morimoto et al. 2000; Isoda 1994).

Unlike in the Gulf Stream or in the Kuroshio Current regions where meanders of the currents pinch-off to form isolated eddies, eddy generation in the Japan Sea is different and varies across various locations within this enclosed sea. . In the sourthern part off the west coast of Japan, eddies originate predominantly due to the interaction of the main current, the Tsushima Warm Current, and bottom topography (Isoda 1996; 1994). On the other hand, off the Korean coast, β-effect (the variation in the Coriolis parameter with latitude) and nonlinearities of the northward flowing western boundary current have been invoked as generation mechanisms of the well-known warm eddy in that area (e.g., Arruda et al. 2004; Lee and Niiler 2010). Around the Peter the Great Bay, several factors seem to be important for the generation of eddies. For example, large eddies are apparently generated by topographic waves propagating along the steep slope, as well as by the meandering and instability of flows in the regions of the Primorye Current and North Korean Current (Ladychenko and Lobanov 2014). These eddies are connected to the stationary currents (Isoda 1994; Ladychenko and Lobanov 2014; Nikitin et al. 2013; Morimoto et al. 2000; Lee and Niiler 2010) and play important roles in physical as well as biological dynamics.

In order to investigate the influence of mesoscale eddies on the biology of the Japan Sea, eddies were identified and tracked based on the methods described above (Figure 1.2). Anticyclonic eddies have a tendency for larger amplitudes and rotational speeds as compared to cyclonic eddies. The radii of both types of eddies are similar. Similar to the findings of Morimoto et al.(2000), eddies with longer lifetimes are found along the path of the Tsushima Warm Current in the western coast of Japan.This region also corresponds to the highest eddy kinetic energy (Figure 1.2).

In the Japan Sea phytoplankton blooms occur with a remarkable regularity (Yamada et al. 2004). The processes leading to spring blooming of phytoplankton in the Japan Sea are consistent with those described by Sverdrup, namely, the development of seasonal stratification and alleviation of light limitation that enhance the growth of phytoplankton, resulting in an increase in biomass and cell numbers that fuel higher trophic levels. The spatial variations in the timing of phytoplankton blooms appear to be related with the ocean dynamics as well as air-sea interactions, namely the development of stratification in the upper mixed layer, the weakening and strengthening of winds in spring and fall, respectively, the melting of sea ice in the northern parts, wet deposition of Asian dust, and a remote influence of El Niño and La Niña events (Yamada et al. 2004; Jo et al. 2007; 2014; Kim, Saitoh et al. 2000; Kim, Yoo et al. 2007). The inter-annual variability in the timing of spring bloom initiation can also be explained by the shifts in wind speed associated with El Niño Southern Oscillation (Yamada et al. 2004). This spatial and temporal variability of phytoplankton blooms have also been well reproduced by numerical models (Onitsuka and Yanagi 2005; Onitsuka et al. 2007).

Mesoscale eddies are integral part of the Japan Sea dynamics and play an important role in many aspects of the chemistry and biology of the Japan Sea (Ladychenko and Lobanov 2014; Kim et al. 2012; Lim, Son et al. 2012; Hyun et al. 2008). Based on *in situ* data,

Hyun et al. (2008) observed that the warm anticyclonic eddy found in the east coast of Korea may have a significant role in the advection of highly productive coastal upwelled water to the deep areas. The enhanced phytoplankton biomass and production is only observed at the ring of the eddy. High production at the ring of anticyclonic eddies have also been observed in early spring (Lim et al. 2012). Contrasting two years of observations, Kim et al. (2012) also found that phytoplankton distribution and composition in the east coast of Korea can significantly be impacted by the presence of anticyclonic eddies during summer when it becomes an intra-thermocline eddy (Gordon et al. 2002). In addition, mesoscale eddies also impact the distribution of foraging species in different parts of the oceans (Sugimoto and Tameishi 1992; Prants et al. 2014; Logerwell and Smith 2001), suggesting that their influence encompass a wide range of oceanographic processes. Therefore, it is important to advance our knowledge about the impacts of eddies in ocean dynamics and ecosystems in the ocean under the influence of climate change.

1.3. Objectives of this Thesis

This study aims at contributing to the understanding of biophysical processes controlling phytoplankton blooms in temperate oceans. The principal subjects of analyses are the mesoscale cyclonic and anticyclonic eddies and their influence on biology and phytoplankton spring blooms. Given the ubiquity of mesoscale eddies and the fact that they are responsible for most of the energy contained in the dynamics of the ocean, their impact can be anticipated to be significant. However, the limitations in data availability within these features have been a major impediment to our understanding of the biophysical processes in eddies. As mentioned before, the Japan Sea, which has been termed “a miniature ocean”, has circulation features similar to the global ocean in which mesoscale eddy activity is strong. Thus, it provides a good opportunity for investigations of linkages between mesoscale eddy activity and biophysical processes. The objectives of this work are the following:

1. Investigate the dynamics of mixed-layer depth in mesoscale eddies and evaluate the impacts on the initiation timing of spring phytoplankton bloom;
2. Reveal the mechanism of phytoplankton seasonal cycle associated with mesoscale eddies in temperate seas.

1.4. Thesis outline

This work is divided into five main Chapters. The first provides an overview of the mesoscale eddies and their importance in the ocean, a brief description of methods of identification and tracking based on satellite altimeter data, and finally the objectives of this study. In Chapter 2, the influence of mesoscale eddies on the timing of spring phytoplankton blooms is investigated based on satellite and *in situ* data co-located within eddy interiors. The main focus here is the timing of spring bloom initiation associated with mesoscale eddies. Given the limitation of satellite data in resolving the vertical distribution of CHL and the paucity of *in situ* data, a nutrient-phytoplankton-zooplankton-detritus (NPZD) model coupled with a one-dimensional turbulence model is used to simulate the annual cycle of plankton dynamics within the mixed layer of mesoscale eddies in Chapter 3. Finally, Chapter 4 and 5 present the general discussion and synthesis (summary of the major findings and the limitations and suggestions for prospective research) of this work are presented.

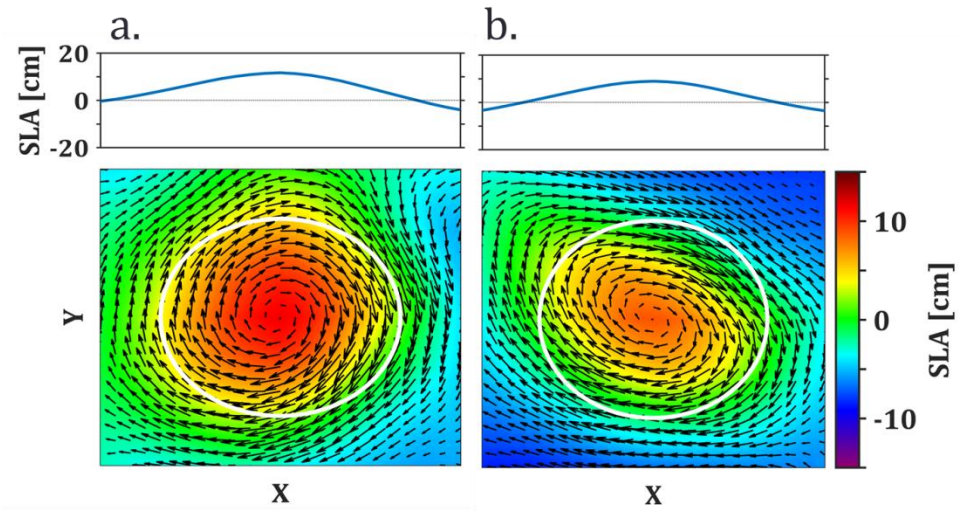

Figure 1.1. Sections of SLA in a clockwise rotating eddy (AE in the northern hemisphere) showing examples of (a) near-circular eddy and (b) eddy with an elliptical shape. Shade indicates SLA and arrows the velocity field. The magnitude of SLA is shown in the upper panels of the figures. X and Y denote longitude and latitude, respectively. A cyclonic eddy (in the northern hemisphere) will have the opposite of the above characteristics.

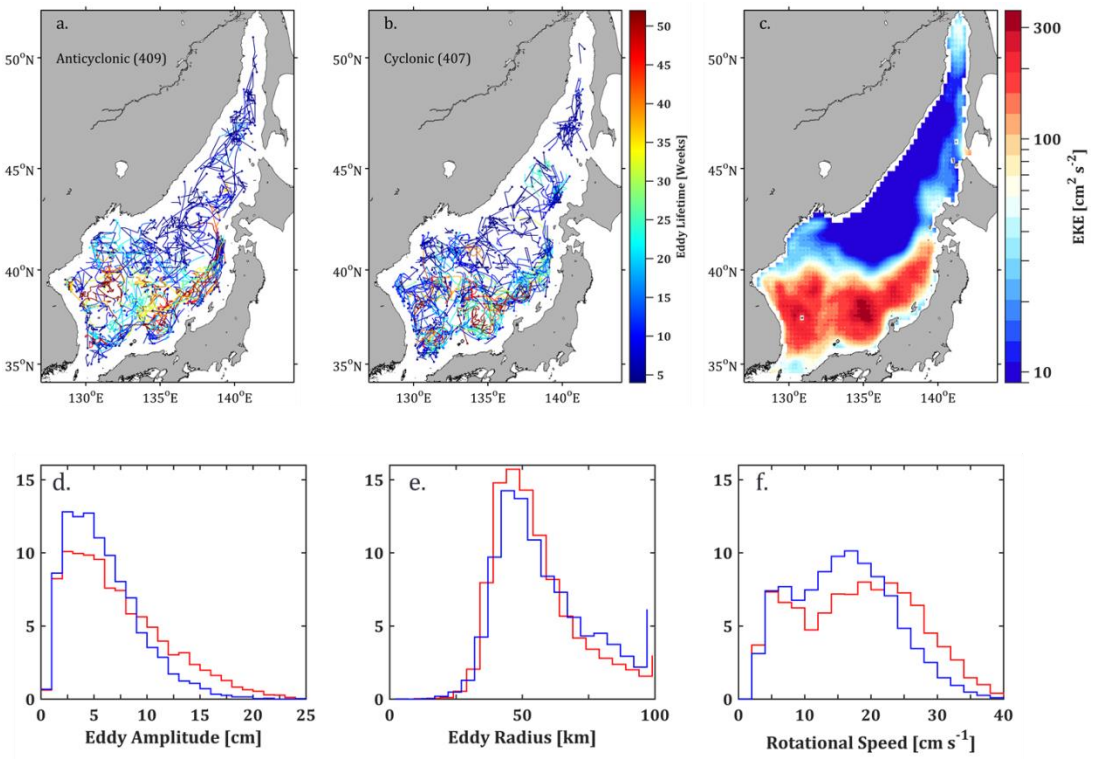

Figure 1.2. Maps of trajectories and statistics of eddies with lifetimes longer than 4 weeks, and Eddy kinetic energy (EKE) map. Trajectories in (a) AEs and (b) CEs. Dots indicate the initial positions identified by the tracking algorithm (section 1.1). The lifetime of each eddy is colour coded. Number of eddy tracks in the map is shown in parenthesis. (c) Eddy kinetic energy (EKE) calculated from satellite geostrophic velocities. Histogram of eddy amplitude (d), eddy radius (e) and rotational speed (f) of anticyclonic (red) and cyclonic (blue) eddies. The SLA data used span the period from September 1997 to April 2012.

Chapter 2

2. Mesoscale Eddies Control the Timing of Spring Phytoplankton Bloom: A Case Study in the Japan Sea

2.1. Introduction

Mesoscale eddies have long been known to induce a large variability of near-surface physico-chemical and biological properties (Gower et al. 1980). They play important roles in regulating primary production in the ocean and its biogeochemical processes (Falkowski et al. 1991; McGillicuddy et al. 1998; Sweeney et al. 2003; Sukigara et al. 2014). Moreover, the existence of eddies have been shown to influence the fishing ground formation (Sugimoto and Tameishi 1992), and the abundance and survival of fish larvae (Logerwell and Smith 2001). They are also known to modify the local vertical density field, thereby impacting the spatial and temporal variations of the mixed-layer depth (MLD). In many parts of the global ocean experiencing winter convective mixing, deeper MLDs occur more frequently within AEs as compared to CEs (Williams 1988; Dufois et al. 2014; Kouketsu et al. 2012; Gaube et al. 2013), and this difference in MLD impacts the seasonality of phytoplankton (Tilburg et al. 2002; Dufois et al. 2016; 2014).

In temperate seas like the Japan Sea, phytoplankton spring blooms (Yamada et al. 2004) occur with a remarkable regularity. Unlike in the oligotrophic subtropical regions where eddies can alleviate nutrient limitation in the euphotic zone through uplift of isopycnals or through vertical mixing (Bibby et al. 2008; Dufois et al. 2016; 2014; Sukigara et al. 2014), temperate waters like the Japan Sea are not nutrient limited before the spring blooms appear so the role of eddies on the seasonal cycle of CHL in temperate regions is poorly understood.

The timing of spring bloom initiation plays an important role in fisheries as well as in carbon export (e.g., Townsend and Cammen 1988; Platt et al. 2003; Koeller et al. 2009; Kahru et al. 2011). The initiation mechanism of the spring bloom has conventionally been explained by the critical depth hypothesis (Sverdrup 1953). This hypothesis assumes phytoplankton growth is light-limited in winter due to deep mixing. In spring near-surface stratification is developed and MLD becomes shallower than the critical depth, resulting in favourable light conditions to induce net phytoplankton growth. This simple hypothesis has served as a framework to build our understanding of the initiation mechanism of the phytoplankton blooms. In recent years, several hypotheses have also emerged (Chiswell et al. 2015; Fischer et al. 2014) building on and extending the critical depth theory (Chiswell 2011; Huisman et al. 1999; Mahadevan et al. 2012; Taylor and Ferrari 2011). Huisman et al. (1999), for instance, attributed bloom initiation to the relaxation of turbulent mixing. This relaxation has been associated with the shutdown of turbulent convection at the end of winter when net cooling subsides (Taylor and Ferrari 2011) and with the decrease in wind stress (Chiswell et al. 2013). Brody and Lozier (2014) compared the role of both wind and buoyancy forcing in the bloom initiation. They predicted a bloom will occur when negative heat fluxes weaken and shift the mixing mechanism from convection to wind driven. Mahadevan et al. (2012) suggested that eddies, in the North Atlantic Ocean, can re-stratify the water column initiating the bloom prior to the onset of ocean heating.

On the other hand, Behrenfeld (2010) proposed an ecological-based framework. In this framework, the interactions between grazers and phytoplankton are crucial to the dynamics of phytoplankton blooms. The disturbance of these predator-prey interactions through dilution effect of mixed layer deepening in winter is pivotal to the initiation of the spring bloom (Behrenfeld 2010; Behrenfeld et al. 2013a). However, the bloom onset mechanism is still a matter of debate (e.g., Behrenfeld and Boss 2014; Chiswell et al. 2015) and the lack of

reconciliation between the different theories (Behrenfeld et al. 2013b; Chiswell 2013) suggests the need for continued consideration of different physical and biological processes controlling bloom dynamics.

In the Japan Sea, a marginal sea of the North Pacific Ocean, mesoscale eddies are ubiquitous but the mechanism of their generation is not completely known (Morimoto et al. 2000). However, around our study region it has been suggested that they are generated by the interactions of the Tsushima Warm Current and bottom topography (Isoda 1994). Phytoplankton spring blooms are observed with a remarkable regularity in this region (Yamada et al. 2004). What is unique here, however, is that the onset of the spring bloom varies spatially starting earlier in the south (Yamada et al. 2004) and this variation has been explained by difference in MLD (Onitsuka and Yanagi 2005). Moreover, the initiation timing of spring phytoplankton bloom has been found to correspond with wind speed (Yamada et al. 2004; Kim et al. 2007). Weak winds were associated with early development of stratification and thus early blooming of phytoplankton, whereas delay in the development of seasonal stratification was associated with strong winds which delayed the start of blooms. In a preliminary study, Lim, Son et al. (2012) explored the short-term variation of both satellite CHL and primary production in early spring associated with AEs. They observed higher CHL and enhanced primary production at the edge of AEs rather than in the centre.

In this study, we evaluated the contribution of both AEs and CEs on the onset mechanism of surface blooms. AEs and CEs are associated with positive and negative MLD anomalies, respectively (McGillicuddy 2016). Therefore, it is reasonable to expect their presence may alter the timing of the spring bloom locally. We investigated how AEs and CEs control the initiation of the spring bloom using satellite CHL along with *in situ* temperature and salinity profiles. We chose the Yamato Basin (YB) region of the Japan Sea, because of its

intense eddy activity (Morimoto et al. 2000). This study area provides a good opportunity for the investigation of interlinks between bloom initiation and mesoscale eddy activity.

2.2. Materials and Methods

2.2.1. Eddy identification and tracking

We used the spatially high-pass filtered version of the global sea level anomaly (SLA) (Chelton et al. 2011b) and geostrophic velocity anomaly data (http://www.aviso.altimetry.fr/), constructed by merging two concurrent altimetry measurements. The data were obtained at ¼º and weekly (7-day) spatial and temporal resolution, respectively. Mesoscale eddies in the YB region (133-139º E and 35-39.5º N), Japan Sea (Figure 2.1), were identified using the geometric eddy detection and tracking algorithm of Nencioli et al. (2010). We also employed extremum of SLA to aid in identifying non-circular eddies that sometimes go undetected by the geometric method. Eddy shape was computed based on the shape of the outer-most closed contour of SLA enclosing an identified centre (Chelton et al. 2011b). Eddies with radii smaller than 40 km were excluded from this analysis. We also computed the speed-based shape, corresponding to SLA with maximum circum-average speed (Chelton et al. 2011b). Eddy tracks were constructed according to the procedure detailed in Nencioli et al. (2010).

2.2.2. Satellite CHL and bloom initiation timing

We obtained CHL data from the GlobColour Project (http://www.globcolour.info/), which provides continuous data sets of merged L3 Ocean Colour products from multiple sensors (SeaWiFS, MERIS, and MODISA) at different spatial and temporal resolutions (http://www.globcolour.info/CDR_Docs/GlobCOLOUR_PUG.pdf). For the purpose of this study, we used daily CHL ($\mathrm{mg\,m^{-3}}$) and photosynthetically available radiation (I_0, $\mathrm{einstein\ (E)\ m^{-2}\ d^{-1}}$) data at ¼º spatial resolution. Merged CHL data from multiple sensors with a weighted average (from April 2002 to December 2011) and simple averaging

(before April 2002) was used. CHL was used as a proxy for phytoplankton biomass. However, as CHL is influenced by light and nutrient-driven changes in intracellular pigment levels more recently satellite estimates of phytoplankton carbon have been used as a measure of phytoplankton biomass (Behrenfeld and Boss 2006; Behrenfeld et al. 2005). These two estimates of phytoplankton have, however, been shown to be highly correlated (Behrenfeld 2010). I_0 was obtained from a simple average of SeaWiFS before June 2002, of MODIS after December 2010, and from a weighted average of SeaWiFS and MODIS from June 2002 to December 2010. I_0 corresponds to the daily mean photon flux density within the visible range (400 to 700 nm) available for photosynthesis by phytoplankton. Variations in I_0, among others, are influenced by seasonal and cloud effects, and those are difficult to be separated. Both daily CHL and I_0 were composited into weekly (7-day) intervals to match the timescale of the eddy dataset. I_{ML} (mean irradiance over the mixed layer) was estimated based on the relationship $I_{\mathrm{ML}} = [I_0/(k\ \mathrm{MLD})](1 - e^{-k\ \mathrm{MLD}})$ (Cole et al. 2015) where k denotes the attenuation coefficient for all I_0 wavelengths obtained from (http://www.globcolour.info/).

To evaluate the influence of mesoscale eddies on the timing of bloom initiation weekly time-series of the geometric mean of CHL (mean of log-transformed CHL) were calculated inside each eddy defined by the speed-based shape. Mean CHL was calculated if pixels with valid data were more than half (> 50%) of the total pixels within the eddy area. The time-series were then transformed back to a linear scale. The linear time-series were used to calculate the timing of bloom initiation by a simple threshold criterion (Siegel et al. 2002) and Gaussian functions (e.g., Yamada and Ishizaka 2006; Zhai et al. 2011).

The Gaussian functions modelled the CHL time-series between January and June using a nonlinear least-square optimization algorithm. The best model fit was selected according to the Akaike Information Criteria (AIC_c) (e.g., Wagenmakers and Farrell 2004; Symonds and

Moussalli 2011). The timing of bloom initiation was defined as the time when CHL reached 20% of the amplitude of the Gaussian function (Zhai et al. 2011).

The threshold criterion identifies the timing of bloom initiation by finding the time when CHL becomes 5% higher than the annual median (Siegel et al. 2002; Brody et al. 2013; Cole et al. 2015). We adopted the same 20% threshold above median similar to the threshold used in the Gaussian function to minimize inconsistency. The use of 5 or 20% as threshold yielded essentially the same result. An additional criterion was that CHL should remain at this concentration for three consecutive weeks to avoid inclusion of a transient increase in CHL not related to the onset of spring bloom. Given that our interest was on initiation timing in mesoscale eddies, the median threshold was calculated from pixels inside the eddy shape over the eddy tracks.

We adopted both Gaussian functions and threshold criterion to avoid the errors caused by gaps in satellite CHL data for determining the timing of phytoplankton bloom initiation (Cole et al. 2012; Ferreira et al. 2014). The Gaussian functions take into account the temporal variation of CHL, thereby reducing the impact of missing data on phenology estimation. However, the functions can at times, fail to correctly model the time-series if there are several peaks or large temporal variation associated with the data. Nonetheless, in this study, both the Gaussian functions and the threshold criterion provided consistent results.

2.2.3. Mixed-layer depth (MLD)

In situ temperature and salinity data were obtained from the US Global Ocean Data Assimilation Experiment (http://www.usgodae.org/), the Japan Meteorological Agency (http://www.jma.go.jp/), the Japan Oceanographic Data Center (http://www.jodc.go.jp/), and the Copernicus Marine Service (http://marine.copernicus.eu/). MLD was calculated based on either density ($\Delta\sigma_\theta = 0.03$ kg m^{-3}) or temperature ($\Delta T = 0.2$℃) threshold (Holte and Talley

2009) from 10 m surface reference level on individual profiles. We used the $0.03\ \mathrm{kg\ m^{-3}}$ as the threshold to define the MLD because it has been suggested to closely follow the depth of active mixing more accurately than the $0.125\ \mathrm{kg\ m^{-3}}$ (Brody and Lozier, 2014). However, for comparison purposes we computed the MLD based on both $0.03\ \mathrm{kg\ m^{-3}}$ (MLD_{03}) and based on $0.125\ \mathrm{kg\ m^{-3}}$ (MLD_{125}). Unless otherwise stated, whenever the term "MLD" is used, it refers to the MLD_{03}. The temperature-based MLD estimation is not significantly different from density-based estimates of MLD (Lim, Jang et al. 2012). MLDs for AEs and CEs were calculated by finding the profiles inside the eddy areas which were defined by the outermost closed contour of SLA.

2.2.4. Air-sea heat flux data

The global dataset of the objectively analysed air-sea fluxes (http://oaflux.whoi.edu) at 1º and daily spatial and temporal resolution, respectively, was linearly interpolated onto 0.25º and composited to weekly datasets. The net heat flux (Q_0) data was available through 2009. Thus, we used data in the period 2002-2009. The mean Q_0 inside eddies was averaged in a similar way to CHL but without log-transformation. Q_0 is positive downward, i.e., ocean heating.

2.3. Results and Discussion

We analysed both AEs and CEs in the YB region from winter (January-February) to spring/early summer (May-June) in 2002-2011. In total, 19 eddies, 11 AEs and 8 CEs, with lifetimes ≥ 17 weeks were analysed. Each year, roughly one eddy of each type was observed at the study site with more AEs events than CEs.

2.3.1. Bloom initiation based on weekly composites of MLD and satellite CHL

We start with a description of the winter conditions in the AEs and CEs. CHL composites of the 10-year record for both AEs and CEs were characterized by low CHL

(< 0.50 mg m^{-3}) with relatively larger temporal variation in CEs (Figure 2.2a). CHL was generally lower in AEs (~ 0.30 mg m^{-3}), with deep MLD (~100 m, Figure 2.2c), whereas it was relatively higher (~ 0.47 mg m^{-3}) in CEs with shallow MLD (50 m, Figure 2.2c). The variation in CHL and MLD in CEs in winter was negatively correlated (Figure 2.2), particularly prior to the bloom onset.

After the bloom initiation, CHL in the CEs increased to > 1.0 mg m^{-3} with some fluctuations while the MLD shoaled. Most importantly, the initiation of the bloom in CEs appeared before the end of winter cooling ($Q_0 < -100$ W m^{-2}, Figure 2.2b).

A different situation prevailed in the AEs. The mixed layer reached depths greater than 100 m between February and March (Julian Day (JD) 43-50 and 71-85, respectively), while CHL increased only slightly (Figure 2.2). The small increase might reflect the high CHL around eddies as seen in Figure 1.1. CHL however, increased further with rapid shallowing of MLD from > 100 m in late March to < 50 m in early May. This shallowing of MLD in AEs was close to the end of winter cooling when Q_0 switches into net heating of the ocean (Figure 2.2c), thus creating conditions for stratification of the water column in the interior of the eddies.

At the time of bloom onset, the average I_0 (I_{ML}) was about 24 (5.6) E m^{-2} d^{-1} in CEs and 32 (2.2) E m^{-2} d^{-1} in AEs (Table 2.1). I_{ML} was calculated on the assumption that MLD approximates the turbulent layer. However, this approximation can fail when this layer is much shallower that the MLD (e.g., Brainerd and Gregg 1995) and this has impacts I_{ML} on estimate. The difference in I_{ML} between AEs and CEs was mostly related to the depth of the mixed layer because the temporal variation in I_0 was similar (Figure 2.2c and d) and, in this area, *k* changes in relation to CHL, i.e., they are positively correlated. Thus, even though

CHL increased with time, I_{ML} of CEs increased due to a decrease in MLD, whereas I_{ML} in the AEs was almost constant during the deepening phase of MLD.

The highest mean CHL ($\sim$2.0 mg m^{-3}) was observed in spring around JD 100 (early April) in both AEs and CEs and earlier peak was generally observed in CEs. After the spring peak of CHL, the pattern of CHL decline was similar for eddies, likely caused by nutrient depletion and/or zooplankton's grazing within the mixed layer (Mann and Lazier 2005). Further stratification also resulted in much shallower MLDs (< 50 m) which were comparable in both AEs and CEs. A schematic that explains the spring bloom initiation in eddies is provided in Figure 2.4.

Our analysis based on the threshold criterion suggests that the spring bloom was on average initiated on JD 57 (late February) in CEs and about three weeks later (around JD 81, late March) in AEs. On the bloom initiation, CHL (MLD) was about 0.63 mg m^{-3} (40 m) and 0.49 mg m^{-3} (161 m) in CEs and AEs, respectively (Figure 2.2, Table 2.1). Conditions at the bloom initiation based on both the Gaussian functions and the threshold criterion were similar (Table 2.1).

2.3.2. Physical forcing and bloom initiation in eddies

The relationship between CHL and physical parameters (MLD, Q_0, and I_0 and I_{ML}) was examined (Figure 2.4) to obtain a better understanding of the mechanisms responsible for the distinctive timings of bloom initiation in both types of eddies described in the preceding section. In CEs, MLD was always shallower than 100 m (Figure 2.2c and Figure 2.4e). It is worth noting that mean winter MLD of 50 m was approximately in the similar range to the euphotic zone (Figure 2.5) and changed only a little with Q_0, especially around zero (Figure 2.4h). Even if surface phytoplankton is being strongly mixed by turbulent convection, the increase in I_0 would improve the light conditions within the shallow MLD. Indeed, the spring

bloom started earlier while Q_0 was still negative (Figure 2.2c and Figure 2.4f) but after I_{ML} increased to about $5.6\ \mathrm{E\ m^{-2}\ d^{-1}}$. I_{ML} increased as I_0 increased (Figure 2.2d) with a concomitant increase in CHL ($p < 0.001$, Figure 2.4g). This is because the shallowing MLD was favourable for I_{ML} increase despite an increase in k with enhanced CHL. This implies that enhancement in light availability for phytoplankton in the shallow MLD triggered the bloom in CEs even though Q_0 was negative.

In the case of AEs, CHL was low ($< 0.50\ \mathrm{mg\ m^{-3}}$) but increased gradually, even as MLD increased with large variations until Q_0 became positive (Figure 2.1 and Figure 2.4a-d). This suggests that a transport of phytoplankton to the aphotic depth through mixing is probably causing light limitation for growth, as long as $Q_0 < 0$. After Q_0 became positive, the MLD shallowed and CHL rapidly increased. This situation where a rapid decrease in MLD as Q_0 turns positive is well evident in Figure 2.4d. The most significant increase in CHL ($\gg 1\ \mathrm{mg\ m^{-3}}$) right at or after $Q_0 = 0\ \mathrm{W\ m^{-2}}$ suggests an important role of the depth of turbulent mixing in controlling bloom initiation in AEs which is consistent with the hypothesis of the shutdown of turbulent convection as a trigger of phytoplankton blooms (Taylor and Ferrari 2011; Ferrari et al. 2015).

I_0 at bloom initiation was higher in AEs ($32\ \mathrm{E\ m^{-2}\ d^{-1}}$) as compared to CEs ($24\ \mathrm{E\ m^{-2}\ d^{-1}}$, Table 2.1), and yet I_{ML} was much lower in AEs [$2.2\ \mathrm{E\ m^{-2}\ d^{-1}}$ ($\sim 5.5\ \mathrm{W\ m^{-2}}$)] than in CEs [$5.6\ \mathrm{Ein\ m^{-2}\ day^{-1}}$ ($\sim 14\ \mathrm{W\ m^{-2}}$)]. This difference in I_{ML} clearly demonstrates the importance of the depth of mixing in controlling the light exposure of phytoplankton within MLD of eddies. Consequently, with I_{ML} increasing to $\sim 14\ \mathrm{W\ m^{-2}}$ it is understandable why blooms were triggered earlier in CEs, despite negative Q_0. The I_{ML} (Platt et al. 2010; Zhai et al. 2011) calculated within the MLD (not actual mixing depth) was much lower in the AEs than in CEs. It is expected that the actual I_{ML}, which phytoplankton

was exposed to, was higher because the turbulent mixing layer can be shallower than MLD when Q_0 becomes positive.

Our results revealed that the spring bloom was initiated earlier in CEs as compared to AEs. The time lag in the bloom initiation between the two types of eddies generally corresponded to the differences in MLDs and is consistent with the classical critical depth hypothesis. However, whilst the critical depth hypothesis predicts blooms to occur when the depth of the mixed layer becomes shallower than the critical depth, in this study we observed the MLDs in CEs were originally shallow, and the earlier blooms in CEs were largely attributed to increases in I_0 which resulted in increased I_{ML}. The deep MLD observed in AEs, which seemed to delay the bloom initiation, indicates that the bloom initiation occurred following improved light exposure due to the relaxation of convective mixing at the end of the cooling season. This is evident from the increase in CHL as Q_0 values became positive. These results show how mesoscale eddies can play an important role in regulating the temporal variability of bloom onset in the Japan Sea.

The alleviation of light limitation in spring is known to trigger the net growth of phytoplankton as a bottom-up mechanism (e.g. Chiswell et al. 2015). MLD of over 100 m in AEs would be sufficient enough to delay or halt the spring bloom due to light limitation unless turbulence is weakened at the near surface. In contrast, the disturbance-recovery theory proposed by (Behrenfeld et al. 2013a) suggests that the bloom is initiated in winter when phytoplankton-grazer interactions are disrupted by physical mixed layer deepening. During spring, parallel increases in phytoplankton-specific division and loss rates then maintain the subtle disruption in food web equilibrium that ultimately yields the spring bloom climax.

This top-down mechanism of bloom initiation is based on an inventory of mixed layer integrated values and estimates of biomass accumulation rates (Behrenfeld 2010) that have sparked a debate (Behrenfeld et al. 2013b; Chiswell 2013). Although no vertical CHL concentrations within MLD of the examined eddies are available, we estimated the rates of accumulation following Behrenfeld (2010) (Figure 2.5).

In CEs, the pattern of integrated CHL is in general similar to that of surface values and the peaks of surface and integrated CHL were very close (Figure 2.5). For shallow MLD in the range of the euphotic depth, the dilution effects of mixed layer deepening are expected to be small and light to be more important for the bloom initiation as it enhances phytoplankton growth within the mixed layer, thereby, offsetting the grazing pressure. In this case, I_0 is the main factor triggering the initiation of the bloom as we suggested above.

In AEs, deepening of MLD corresponds to an increase in integrated CHL, and this situation may support a top-down interpretation of the winter bloom initiation (Behrenfeld 2010). However, in the surface layer, the increased CHL in relation to Q_0 is a consequence of the shutdown of convective mixing which triggers surface phytoplankton blooms. The above difference indicates the possibility of separation between shallow and deep waters and inhomogeneity of CHL within MLD. Moreover, the MLD used in this study was a combination of MLDs in eddies in different years. For this reason, the large variation observed during the deepening phase could not be examined in detail. Thus, further research would be required to evaluate the disturbance-recovery hypothesis, although the importance of Q_0 for the bloom initiation in AEs is clear.

As mentioned above (in section 2.2.3), our estimated MLD, using $0.03\ \mathrm{kg\ m^{-3}}$ (MLD_{03}) threshold, was much shallower than the one using $0.125\ \mathrm{kg\ m^{-3}}$ (MLD_{125}) threshold (Figure 2.5). The latter follows the depth of the seasonal thermocline while the former might be a

close approximation of the depth of active mixing (Brody and Lozier 2014). In CEs, for instance, if the mixing layer corresponded to MLD_{125} (similar to the one used in Behrenfeld et al. (2013a)), the light would have been limiting at the time when blooms were initiated in CEs because it was deeper than 100 m. In AEs, the timing of maximum MLD for both $0.03\ \mathrm{kg\ m^{-3}}$ and $0.125\ \mathrm{kg\ m^{-3}}$ was close. However, MLD_{03} rapidly shallowed after Q_0 became positive (Figure 2.4d) compared to MLD_{125} (Figure 2.5). Therefore, if MLD_{03}, in fact, approximates the active turbulent layer, it is important for understanding bloom dynamics.

In certain regions like the Gulf of Alaska (Crawford et al. 2005), the Gulf Stream and the Leeuwin Current region (McGillicuddy 2016), eddies are known to trap and transport offshore coastal waters rich in nutrients and phytoplankton. This phenomenon does not seem to be a dominant process in our study region because the AEs and CEs studied here appear to be randomly distributed (Figure 2.6). They are generally formed south of the subpolar (south of 40^{o}N) and not from systematic source regions like in the case of the Leeuwin Current region and the Gulf Stream.

2.4. Summary and conclusions

Satellite CHL and *in situ* data were used to investigate the influence of mesoscale AEs and CEs on the timing of spring phytoplankton bloom initiation around the Yamato Basin in the Japan Sea, for the period 2002–2011. Thus, this study has shown the role of mesoscale eddies on the timing of the spring phytoplankton bloom initiation in the Japan Sea. First, we confirmed observations that modulation of the mixed layer by mesoscale eddies resulted in deeper (shallower) MLDs in AEs (CEs). Second, we have demonstrated that this difference in MLD has significant implications for bloom initiation. Our study shows that the depth of mixing controlled bloom initiation in eddies. For CEs, on account of their shallow MLD, bloom initiation appears to be controlled by bottom-up processes described by Sverdrup (1953), i.e. shallowing of the MLD and increasing I_0. In contrast, alleviation of light

limitation in AEs was related to relaxation of convective mixing. Thus, in this case, the trigger of phytoplankton blooms appears to be the shutdown of convection (Taylor and Ferrari 2011; Ferrari et al. 2015) because bloom initiation commenced when $Q_0 = 0\ W\ m^{-2}$ despite deep MLD. This means that vertical mixing was suppressed at the end of winter and that phytoplankton growth conditions were enhanced causing a bloom to occur.

To the best of our knowledge, this study provides the first insight into the effects of long-lived (≥ 17 weeks) mesoscale eddies on the timing of spring bloom initiation. In temperate waters, early blooms may enhance the export of organic material to the bottom particularly when they appear in cold waters, when metabolic rates of zooplankton are slow, and consequently grazing pressure is reduced. Conversely, late blooms, occurring in warmer waters, can enhance grazing rates and zooplankton growth which in turn supports high trophic species (Townsend and Cammen 1988; Townsend et al. 1994; Hunt et al. 2002). Therefore, the presence of eddies may affect not only primary producers but also the abundance of foraging fish as well as marine ecosystems dynamics. While our study focuses on the YB in the Japan Sea, we believe that this phenomenon is common to other temperate oceanic regions where eddies proliferate.

Table 2.1. Mean conditions at the onset of the spring bloom in AEs and CEs.

Parameter		Start date [day]	CHL [mg m^{-3}]	MLD [m]	Q_0 [W m^{-2}]	I_0 [E m^{-2} d^{-1}]	I_{ML}
Threshold criteria	AEs	81 (12)	0.49 (0.17)	161 (52)	–13 (35)	32 (3.8)	2.2 (1.1)
	CEs	57 (13)	0.63 (0.17)	40 (18)	–133 (34)	24 (2.6)	5.6 (3.1)
Gaussian functions	AEs	87 (18)	0.61 (0.17)	111 (40)	1.8 (38)	35 (3.8)	3.5 (1.7)
	CEs	51 (28)	0.68 (0.15)	45 (18)	–141 (56)	23 (2.1)	4.5 (2.0)

Note: Values are shown as mean (standard deviation). The timing of bloom initiation in AEs and CEs is different at 95% confidence interval.

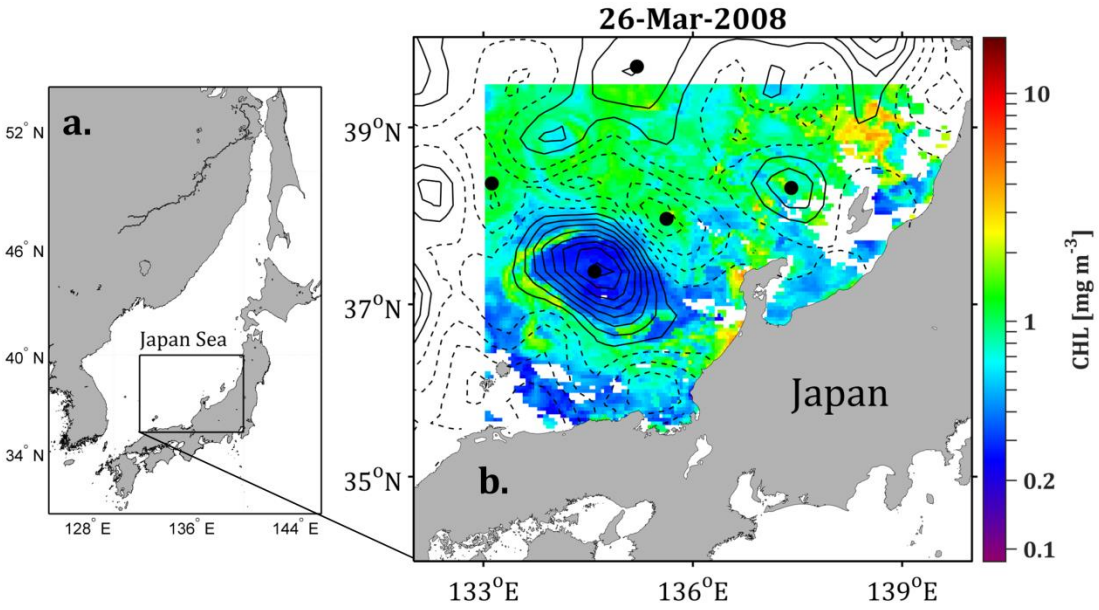

Figure 2.1. Study area in (a) the Japan Sea and (b) the enlarged map around YB. Distribution of SLA contours overlaying colour shading of the concentration of CHL for the week starting on 26 March 2008. Solid and dashed contours represent AEs and CEs, respectively. Dots indicate identified eddies in the current week. Note the low CHL in the interior of AEs in early March.

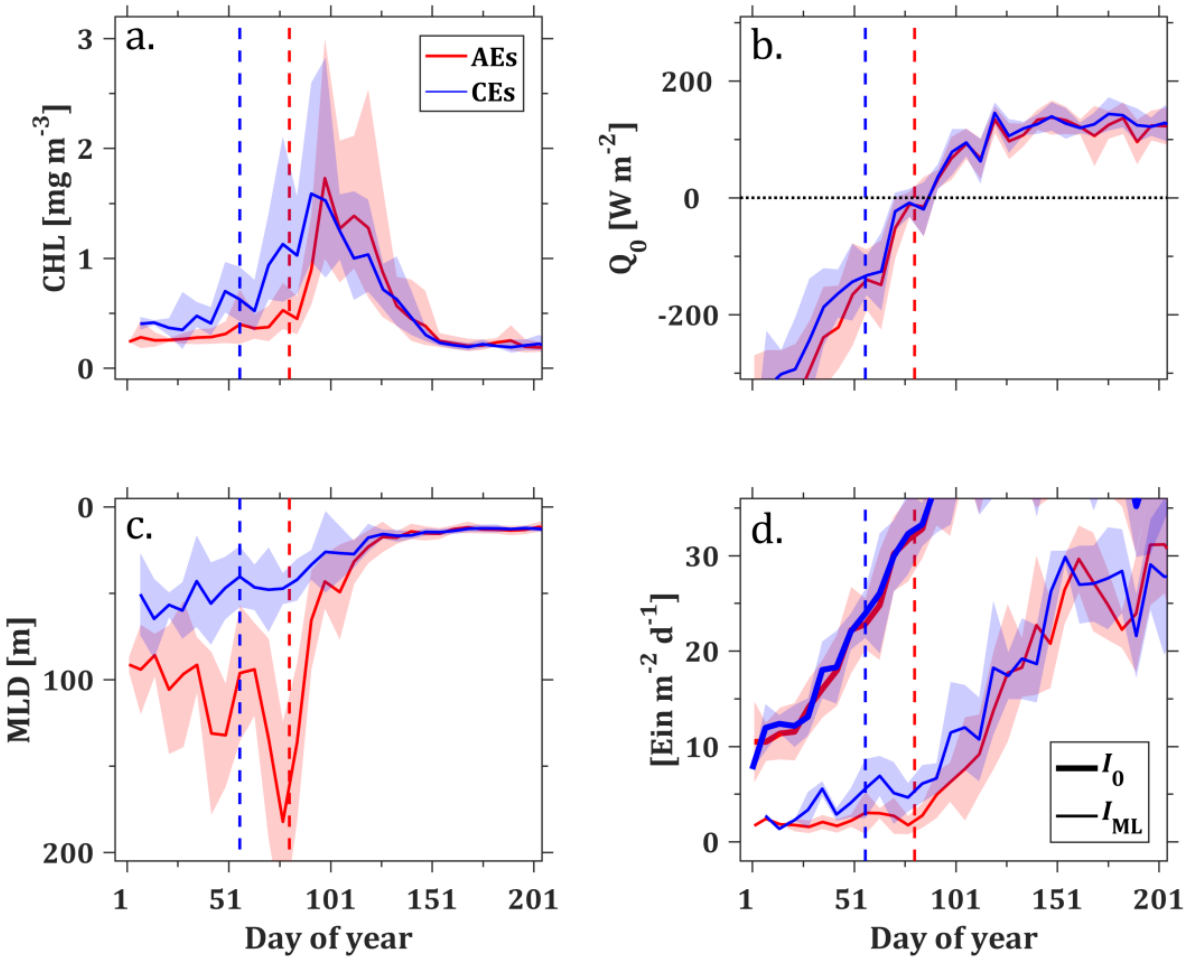

Figure 2.2. The 10-year composites in AEs (red) and CEs (blue) of (a) CHL, (b) Q_0, (c) MLD, and (d) I_0 (thick line) and I_{ML} (thin line) time series. Lines and shades are the mean and standard deviation, respectively. Vertical dashed lines denote the mean timing of bloom initiation.

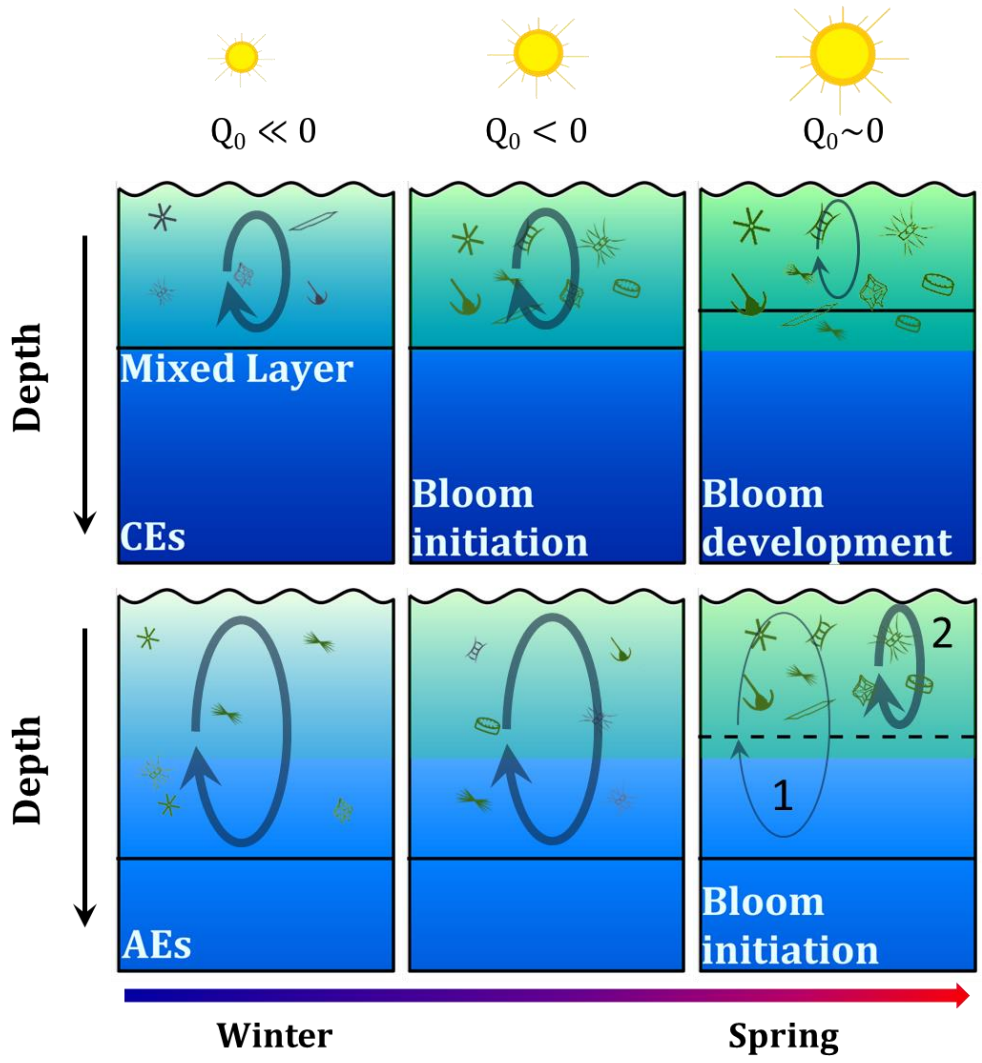

Figure 2.3. Idealized mechanism of spring bloom initiation in eddies. AEs: convectively-driven mixing moves phytoplankton out of the euphotic depth during deep winter mixing. This mixing result in dilution and therefore decrease in phytoplankton and grazer concentration within the mixing layer. While this mixing decrease the near-surface CHL in part because of dilution and decreased light exposure, mixed-layer integrated CHL may start increasing because the dilution effect decreases the grazing pressure on phytoplankton and mixed-layer net population growth become possible. At end of cooling (net heat flux $Q_0 \sim 0$ W m^{-2}), photosynthetically active radiation (I_0, E m^{-2} d^{-1}) have increased considerably and either (1) shallow mixing or (2) slow rate of mixing allow phytoplankton to be retained in the

near-surface for long enough so that surface phytoplankton concentration increases rapidly and bloom occurs. CEs: dilution is not strong enough to dilute prey and predators in winter because mixing is always within shallow layer and thus with increase in I_0, the light condition becomes improved in the shallow mixed layer and both surface and mixed-layer phytoplankton concentration start increasing before Q_0 switches to positive. Note that this description of bloom initiation corresponds to surface bloom as detected by satellites with possible incorporation of the dynamics of blooms within the mixed layer.

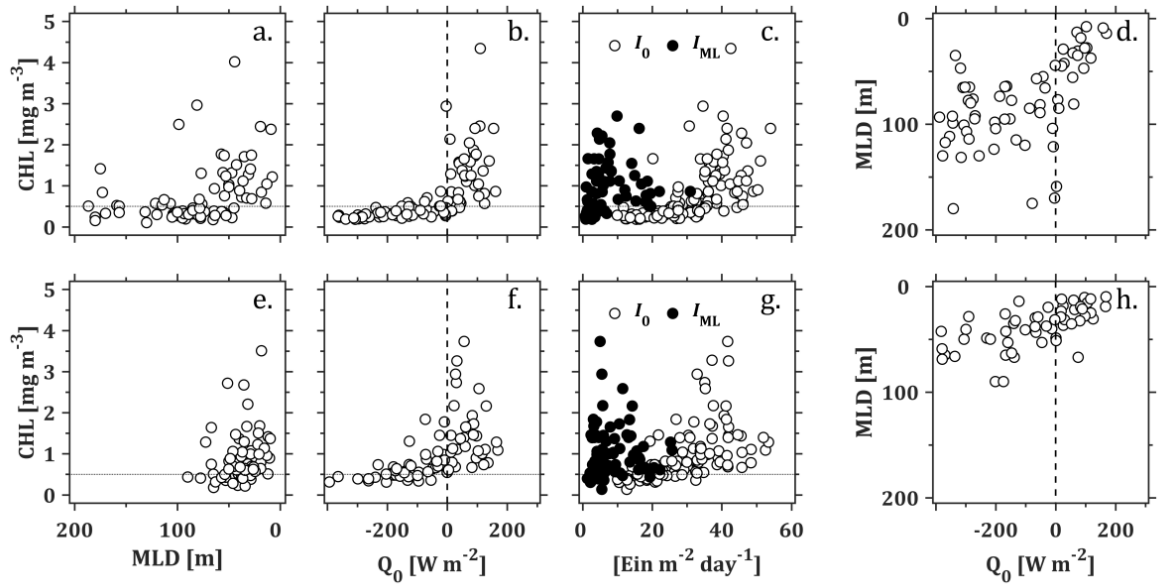

Figure 2.4. Scatterplots of CHL versus MLD, Q_0, and I_0 and I_{ML} (black dots) in (a–c) AEs and (e–g) CEs over the period 2002–2011 (2002–2009 for Q0). Scatterplots of MLD versus Q_0 in (d) AEs and (h) CEs. The horizontal line of 0.50 mg m^{-3} is shown (a–c, e and f) as a reference to winter CHL level. Also, vertical reference line of Q_0 = 0 W m^2 is shown (b, d, f, and g).

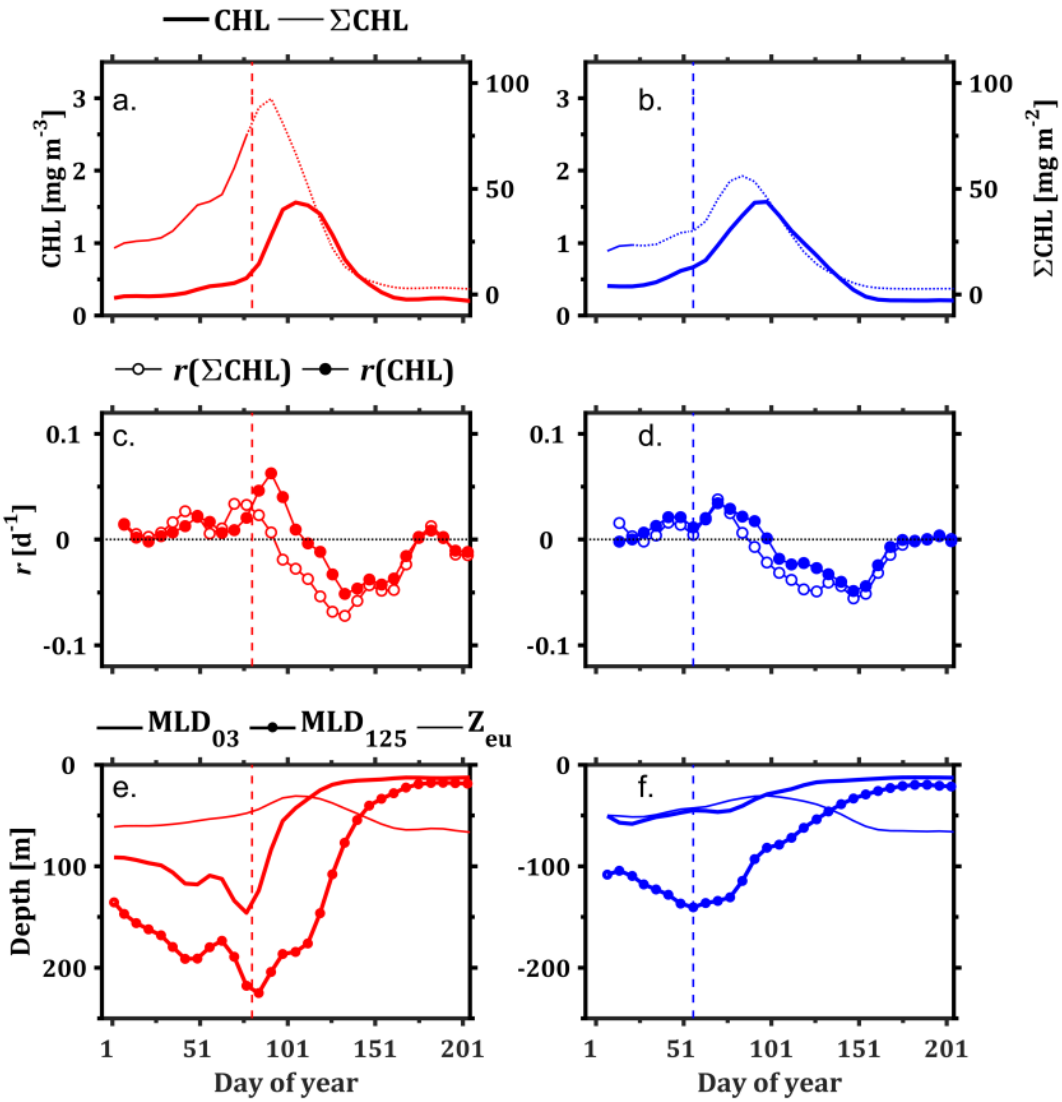

Figure 2.5. Mean CHL concentration, rate of biomass accumulation (r), MLD03 and MLD125, and the euphotic depth (Zeu, the depth at which light intensity became 1% of surface value) in (a, c, e) AEs and (b, d, f) CEs, respectively. Vertical dashed lines (blue and red) denote the mean timing of bloom initiation. Mixed-layer (MLD_{03}) integrated CHL($\sum$CHL) is shown as dotted line during period of MLD shallowing. Rate of accumulation (r) is calculated according to the equations (1) $r = \ln(\sum \mathrm{CHL}_1/\mathrm{CHL}_0)/\Delta t$ if MLD_{03} is deepening and deeper than Z_{eu} or (2) $r = \ln(\mathrm{CHL}_1/\mathrm{CHL}_0)/\Delta t$ if MLD_{03} is shoaling or shallower than Z_{eu} (Behrenfeld, 2010). CHL_0 and CHL_1 are CHL levels at the initial and after the time interval Δt=7 (seven days). Mixed-layer integrated CHL is determined as (CHL ×

MLD_{03}). CHL and MLD data was smoothed with a three-point symmetric moving average filter prior to calculating *r*.

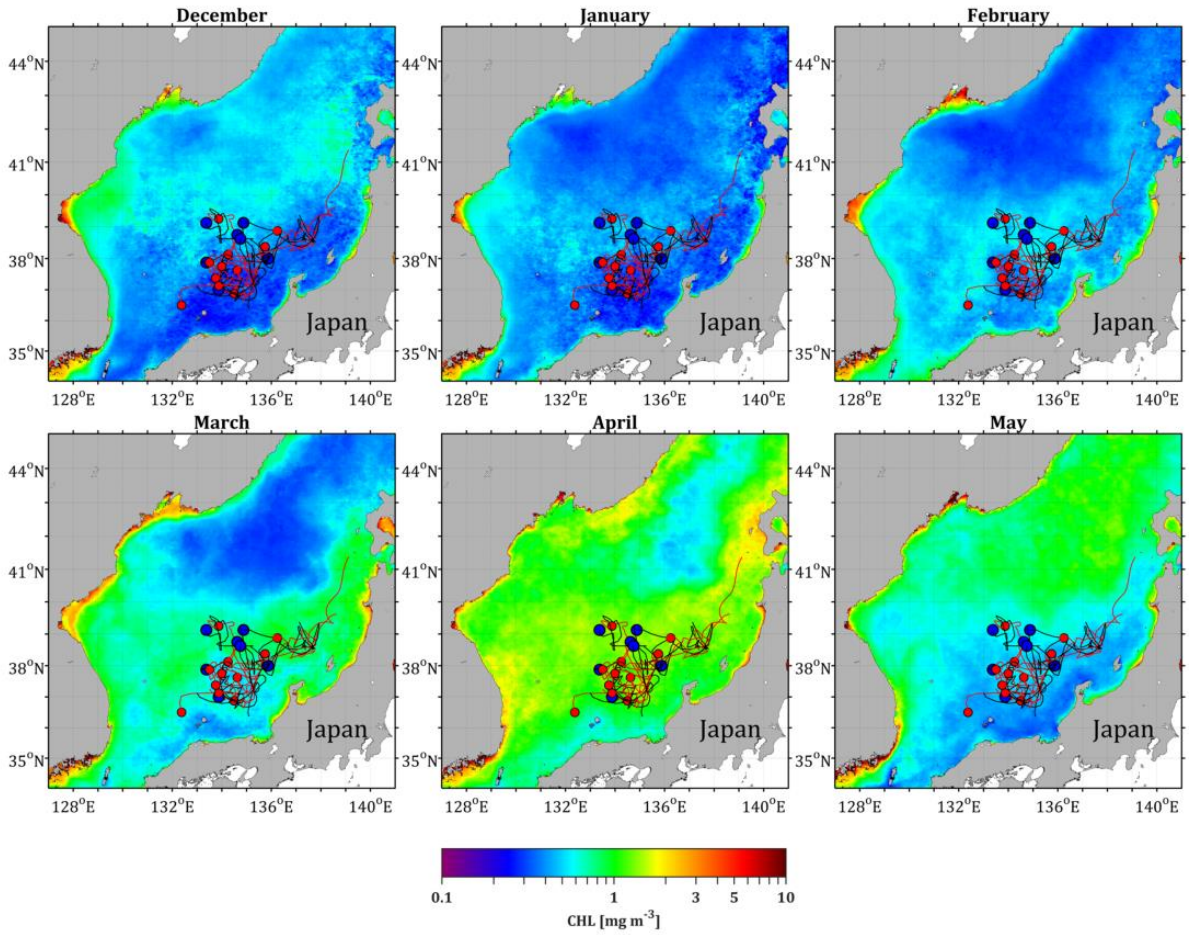

Figure 2.6. Monthly composite maps of CHL (December-May, 2002-2011) overlaid with eddy trajectories analysed in this study. Blue and red circles indicate the initial positions while black and red lines show the trajectories of cyclonic and anticyclonic eddies, respectively.

Chapter 3

3. One-Dimensional Turbulence-Ecosystem Model Reveals the Triggers of the Spring Bloom in Mesoscale Eddies

3.1. Introduction

Mesoscale eddies play an important role in the transport of heat and freshwater as well as in the upper-ocean circulation. Therefore, they contribute on the regulation of global heat budget and climate (Dong et al. 2014; Zhang et al. 2014). Moreover, the presence of mesoscale eddies is also known to significantly disturb the vertical and horizontal distribution of biological and chemical properties (McGillicuddy and Robinson 1997; McGillicuddy et al. 1998). Consequently, their influence also extends to marine productivity and biogeochemical processes (Falkowski et al. 1991; McGillicuddy et al. 1999; Sukigara et al. 2014) and also on fishing ground formation (Sugimoto and Tameishi 1992) and the abundance and survival of fish (Logerwell and Smith 2001).

The spring bloom, a recurring phenomenon observed in temperate ocean, is an important event for higher trophic levels and carbon export (e.g., Koeller et al. 2009; Platt et al. 2003; Omand et al. 2015; Kodama et al. 2018). The role of physical drivers in controlling the spring bloom event has been central to the discussion of the mechanism initiating a bloom since the early works (e.g., Riley 1942; Sverdrup 1953). Sverdrup (1953) provided a quantitative description of the bloom initiation mechanism in which light exposure of the winter phytoplankton is decreased by the deep mixing that circulates phytoplankton over this deep layer resulting in light-limited growth during winter. In spring, near-surface stratification is developed and the mixed layer decreases below the critical depth. This creates

favourable light conditions for rapid phytoplankton division which exceeds losses and so induce net phytoplankton growth thus initiates a bloom.

This simple hypothesis has been fundamental to improving our understanding of the initiation mechanism for phytoplankton blooming. However, this view of the bloom initiation has been questioned in part due to blooms observed in the absence of stratification (e.g., Townsend et al. 1992) and because the role of grazers, suggested to be pivotal for the initiation of phytoplankton blooms (e.g., Behrenfeld 2010), are implicit in Sverdrup's mechanism and generally have been ingonered in subsequent testaments to this model (Smetacek and Passow 1990). For the blooms initiated in the absence of water column stratification, Huisman et al. (1999) suggested a critical turbulence hypothesis mechanism in which blooms develop if turbulent diffusion falls below a critical turbulence which has been subsequently associated with shutdown of turbulent convection at the end of winter when net cooling subsides (Taylor and Ferrari 2011).

On the other hand, zooplankton grazing has been known to play a role in the regulation of phytoplankton seasonal cycle (Riley 1946). Question of whether it is the key to bloom initiation in temperate regions or not has remained elusive in part due to limited information of *in situ* grazing rates. Some literature have found evidence for net winter population growth due to decreases in grazing (e.g., Yoshie et al. 2003; Behrenfeld 2010; Behrenfeld et al. 2013). However, the importance on initiating a bloom remains to be confirmed in different regions of the global ocean where reccurent spring blooms occur.

Maúre et al. (2017) explored the role of physical processes (mesoscale anticyclonic and cyclonic eddies) in the spring bloom initiation. Taking the Japan Sea as a case study, they found that the onset mechanism for surface blooms was different in anticyclonic eddies (AEs) and cyclonic eddies (CEs). The difference in the timing of bloom initiation was attributed to the difference in the mixed-layer depth (MLD). Earlier blooms were observed in shallow

mixed-layer CEs and were triggered by increased averaged light, whereas in the deep mixed-layer AEs the alleviation of light limitation was associated with the relaxation of convective mixing.

In this study, we extend the work in Chapter 2 and apply a 1D coupled turbulence physical-biological model to investigate the spring bloom initiation associated with AEs and CEs. The 1D paradigm does not take into account the horizontal processes associated with the dynamics of eddies. However, in the case of nonlinear eddies capable of trapping water parcels in their interior as they propagate (Chelton et al. 2011), their interior can be considered an isolated environment from the surroundings and a 1D model may suffice in understanding the processes associated with the dynamics of their mixed layers and biology. Moreover, under light limited conditions typical of pre-bloom period, the 1D paradigm is useful in explaining the conditions leading to a bloom (McGillicuddy et al. 1995), and this approach have been useful in testing and evaluating the different factors playing a role in the initiation of phytoplankton blooms (e.g., McGillicuddy et al. 1995; Yoshie et al. 2003; Kuhn et al. 2015; Lévy 2015).

The objective of the study is to investigate the importance of turbulent convective mixing on bloom initiation in AEs and CEs based on model simulation. Therefore, we first simulated the ecosystem dynamics associated with mesoscale eddies through the use of 1D coupled turbulence physical-biological model forced by realistic atmospheric conditions averaged in the interior of eddies. Furthermore, to understand the differences in the timing of the bloom initiation processes playing a role in initiating the bloom in AEs and CEs were analysed. Using the model outputs, the potential role of grazing on bloom initiation was also evaluated.

3.2. Materials and Methods

3.2.1. Model Design and Numerical Experiments

3.3.1.1 Mixed Layer Model

The mixed-layer model used was a 1D turbulence closure model (Mellor and Yamada 1982) applied to a large eddy simulation (LES) of a resonant inertial response of the mixed-layer to wind forcing (Furuichi et al. 2012). The model is an improvement over the Nakanishi and Niino, NN, (Nakanishi and Niino 2009) version of the Mellor-Yamada (MY) turbulence closure model. The MY model is often criticised for having shallow mixed-layers and associated strong warming of surface temperatures during summer (Mellor 2001). On the other hand, the NN model is known to overestimate the development of mixed-layer features such as strong entrainment at the base of the oceanic mixed-layer resulting in decreased sea surface temperature (Furuichi et al. 2012). Furuichi et al. (2012) modified NN by strongly decreasing the NN turbulent length scale. The length scale was allowed to decrease with increasing density stratification. Details of the model can be found in Furuichi et al. (2012). The governing equations are defined below.

$$\left(\frac{\partial}{\partial t} + \boldsymbol{u} \cdot \nabla\right)\boldsymbol{u} + \boldsymbol{f} \times \boldsymbol{u} = \frac{\partial}{\partial z}\left(\nu \frac{\partial \boldsymbol{u}}{\partial z}\right), \tag{3.1}$$

$$\frac{\partial \boldsymbol{F}}{\partial t} = \frac{\partial}{\partial z}\left(\kappa \frac{\partial \boldsymbol{F}}{\partial z}\right), \tag{3.2}$$

where t is time, $\boldsymbol{u} = (u, v)$ is the two-dimensional velocity vector, f is the Coriolis parameter, z the water depth (positive upward), and ν is the eddy viscosity. $F = (T, S, TKE, u, v)$ corresponds to the five-model variable, namely temperature (T), salinity (S), turbulent kinetic energy (TKE), and the last two are the above-mentioned velocities. κ is the eddy diffusivity.

Shortwave radiation (Q_S), net heat flux (Q_0) and wind stress (τ) were applied as surface boundary conditions for the mixed-layer model. Q_S has a profile of downward penetration of solar radiation as a function of depth formulated according to the absorption law (Paulson and Simpson 1977). At the surface boundary, modelled temperature is forced by Q_0 and defined as:

$$\left(\frac{\partial T}{\partial t}\right)_{z=0} = \frac{Q_0}{\Delta z \rho_0 c_p}, \tag{3.3}$$

where water temperature is relaxed at the surface towards a climatic sea surface temperature (T_S^{clim}) (Barnier et al. 1995) according to,

$$T_{z=0} = T(z=0) - \Delta t * \left(T_S^{\text{clim}} - T(z=0)\right) * 4\sigma\left(T_S^{\text{clim}}\right)^3 / \Delta z c_p \rho_0 \tag{3.4}$$

where $\sigma = 5.67 \times 10^{-8}\ \text{Wm}^{-2}\text{K}^{-4}$ is the Stefan-Boltzmann constant. This correction term only considers the longwave radiation term. The net longwave radiation at the surface of the ocean is the sum of the downward radiation from the atmosphere and the upward radiation from the ocean surface. For a prescribed atmosphere, only the latter depends on the ocean sea surface temperature (SST). It accounts for the upward radiation from the ocean surface assuming the ocean radiates as a black body (Barnier et al. 1995). While in Furuichi et al. (2012) a resonant wind stress was applied, for this study a realistic wind stress forcing obtained and averaged in eddies was applied. The integration was carried out using combined forward-backward Euler schemes with $\Delta t = 240$ s and a leap-frog scheme with $\Delta t = 120$ s. The model has a vertical resolution of $\Delta z = 1$ m and maximum depth of 400 m.

Three physical depths used in later sections are now defined. The first of the three is the mixed-layer depth (MLD). It was defined as the depth at which density increases 0.03 kg m^{-3}

from the surface value and was calculated from the model density output. The second is the depth of active turbulence or the turbulent layer depth (TLD). This was defined as depth at which eddy diffusivity (κ) is larger than a certain threshold (10^{-2} m^2 s^{-1}). Values larger than the threshold κ are considered to represent convective mixing condition (e.g., Lévy 2015). And the third is the euphotic layer depth (Z_{eu}). This layer depth was defined as where the light field in the water column (I_z) decreases to 1% relative to surface irradiance (I_0).

3.3.1.2 The Ecosystem Model

The ecosystem model used is an NPZD (dissolved inorganic nitrogen (DIN), phytoplankton (PHY), zooplankton (ZOO), and detritus (DET)) model that has been previously successfully applied to simulate the ecosystem dynamics of the Japan Sea (Onitsuka et al. 2007; Onitsuka and Yanagi 2004). In this study, the NPZD model is coupled to a 1D turbulence closure model that resolves the temporal and vertical variation of diffusivity and was applied to investigate the differences in ecosystem dynamics between AEs and CEs. Assuming that the differences are mainly caused by physical conditions in eddies, satellite and *in situ* data obtained and averaged in the interior of eddies were used as surface atmospheric forcing and to initialise both physical and biological models. The model simulates the dynamics of eight biological processes controlling the different lower trophic level interactions (Figure 3.1). The state variables are modelled according to the following general equation.

$$\frac{\partial C_i}{\partial t} - w\frac{\partial C_i}{\partial z} = \frac{\partial}{\partial z}\left(\kappa\frac{\partial C_i}{\partial z}\right) + B(C_i), \tag{3.5}$$

where C_i is the state variable in the ecosystem model for the ith compartment with $i = (DIN, PHY, ZOO, DET)$, t is the time, w_i is the sinking speed, and $B(C_i)$ represents the

interactions of the four biological compartments and the equations describing the interactions are the following.

Nitrate:

$$B(DIN) = \frac{dN}{dt} = -U_P + (\alpha_z - \beta_z)G_z + RPe^{k_R T} + r_{DN}De^{k_T T}, \quad (3.6)$$

Phytoplankton:

$$B(PHY) = \frac{dP}{dt} = U_P - RPe^{k_R T} + m_P P^2 e^{k_T T} - G_z + w_P \frac{\partial P}{\partial z}, \quad (3.7)$$

Zooplankton:

$$B(ZOO) = \frac{dZ}{dt} = \beta_z G_z - m_Z e^{k_T T} Z^2, \quad (3.8)$$

Detritus:

$$B(DET) = \frac{dD}{dt} = (1 - \alpha_z)G_z + (m_Z Z^2 + m_P P^2 - r_{DN} D)e^{k_T T} + w_D \frac{\partial D}{\partial z}, \quad (3.9)$$

Nutrients are consumed by PHY through uptake to fuel their growth (U_P), and produced through PHY respiration, decomposition by bacteria and ZOO excretion. U_P is limited by the availability of nutrients and light and the maximum growth depend on temperature.

$$U_P = \mu_{\max} \frac{DIN}{K_N + DIN} \frac{I_z}{I_{opt}} \exp\left(1 - \frac{I_z}{I_{opt}}\right) P, \quad (3.10)$$

where $\mu_{\max} = \mu_0 e^{k_T T}$ is the temperature dependent maximum growth (Eppley, 1972), μ_0 is the maximum photosynthetic rate of PHY at 0°C, T the temperature and k_T the temperature coefficient for growth and other temperature dependent processes Eqs. (3.6–3.9). Nutrient limitation (L_N) for growth is modelled by the Michaelis-Menten Kinectics $L_N = \frac{DIN}{K_N + DIN}$, where K_N is the half saturation constant. Light limitation is based on saturating and photo-inhibiting response exponential equation $L_I = \frac{I_z}{I_{\text{opt}}} \exp\left(1 - \frac{I_z}{I_{\text{opt}}}\right)$. I_{opt}, the optimum light, determines the irradiance at the maximum photosynthesis. Light decreases exponentially with depth according to:

$$I_z = I_0 \exp\left(-k_W z - k_P \int_z^0 P dz - k_D \int_z^0 D dz\right), \tag{3.11}$$

where I_0 is the irradiance at the surface exponentially attenuated with depth z by water, PHY, and DET at the rates k_W, k_P, and k_D, respectively. PHY respiration is a function of temperature and exponentially increases with increase in temperature at the rate k_R, the temperature coefficient for respiration.

Zooplankton grazing (G_z) is based on the Ivlev formulation:

$$G_z = g_{\max} \times \max\left(0, 1 - e^{[\lambda(\sigma - P)]}\right) e^{kT} Z \tag{3.12}$$

where the threshold σ determines the lower limit of grazing. Grazing also depends on temperature and the maximum potential grazing is given by $g_{\max}$. ZOO excretes the fraction $(\alpha_z - \beta_z)$ of the total grazing into nutrient pool. Here, α_z and β_z are the assimilation efficiency and growth efficiency, respectively. PHY and ZOO mortalities are channelled into

the DET and part of the dead organic matter is remineralized back into the DIN at the rate r_{DN} and is a function of temperature. Details of the definition of parameters, units, and values used are given in Table 3.1 and are mostly based on those found in Onitsuka et al. (2007) and Onitsuka and Yanagi (2004).

3.3.1.3 Restoration of Temperature, Salinity and DIN

Given the limitations of a 1D experiment in resolving the dynamics of 3D oceanic processes, other studies (e.g., Scott et al. 2011; Kuhn et al. 2015) have applied a restoration term to account for the additional processes not resolved in 1D model such as horizontal advection and diffusion (Moisan and Hofmann 1996).

In our experiment in the Japan Sea, over the year, the annual budget of Q_0 is negative, i.e., net cooling (Figure 3.2). Even with the above SST correction term, the modelled temperature decreases every annual cycle and MLD deepens every year (Figure 3.3). So, in order to circumvent the net cooling associated with Q_0 and to reproduce reasonable mixed layers associated with AEs and CEs, the same restoration term as in other studies (Moisan and Hofmann 1996; Moisan et al. 2007; Scott et al. 2011; Kuhn et al. 2015) was also applied to the profiles of temperature and salinity to compensate for the net cooling of Q_0 and to produce the difference in MLD between AEs and CEs. The restoration term was defined as:

$$\boldsymbol{C_{\mathrm{New}} = C_i + \Delta t * R(C_0 - C_i)}, \tag{3.13}$$

where C_{i} is the model solution for the tracer $i = (T, S)$ at each time step. C_0 is the initial profile of the tracer, C_{New} is the tracer after the restoration. R is the restoration rate (1/270 and 1/120 per days for AEs and CEs, respectively) and $\Delta \mathrm{t}$ is the model integration time step.

The restoration applied in this manner, at each time step the difference between C_i and C_0 is relaxed reducing their difference by a fixed rate of $\Delta t/(270 * 86400)$ s in AEs and

$\Delta t/(120 * 86400)$ s in CEs. About 0.0010% of the difference $(C_0 - C_i)$ is added to C_i in AEs and 0.0023% in CEs. Because the composite Q_0 for 10-year period is smoother than in one specific year, the strength of restoration rate for the experiments along each individual eddy track (2.3) was increased ($\Delta t/(150 * 86400)$ s in AEs and $\Delta t/(60 * 86400)$ s in CEs) to avoid the effects of strong cooling.

The profile of DIN was also similarly restored according to the above procedure. Keeping DIN without restoration, it quickly becomes depleted in surface layers. Instead of restoring the deep layers only, as in other studies (e.g., Scott et al. 2011; Kuhn et al. 2015), we keep the restoration for the whole profile. Doing so, we avoided a decrease to zero in the biological terms during stratified months when DIN is depleted and reasonable levels of background chlorophyll *a* (CHL) concentration in these months could be maintained in agreement with observations. Moreover, the initial condition used for restoration was in October while the vertical profile was still stratified with low DIN in the surface.

The second term of Eq. (3.13) was negative in months of deep MLD and was positive during the shallow MLD stratified months. Therefore, this restoration has no effect on the results obtained during nutrient-replete period prior to bloom initiation which is central to the current study. Moreover, because the restoration for the other biological terms was set to zero, the resulting biological fields are the result of the biological forcing (DIN) rather than restoration (Moisan and Hofmann 1996).

3.3.1.4 Initial Conditions and Surface Forcing

The initial conditions for the physical model (profiles of temperature and salinity) and for the biological model (profiles of DIN, PHY, ZOO, and DET) were obtained from *in situ* observations averaged in the interior of AEs and CEs (Figure 3.4). The details of data compositing method for *in situ* and satellite data sets in the interior of eddies can be found in

Maúre et al. (2017). PHY was converted to CHL based on molar ratios of carbon (C) to CHL, i.e., C: CHL ratio of 50:1 and the Redfield C to nitrogen (N), i.e., C: N ratio of 106:16. ZOO and DET were arbitrarily assigned initial values based on the profile of PHY (PHY/10 for both ZOO and DET).

The physical model was forced by Q_0, Q_S, and τ. Q_0 and Q_S (Figure 3.2) were obtained from the global dataset of the Japanese Ocean Flux Data Sets with Use of Remote Sensing (J-OFURO) project third-generation (J-OFURO3) at daily temporal and 0.25° spatial resolutions (https://j-ofuro.scc.u-tokai.ac.jp). These data were available in the period from 2002 to 2013. Prior to 2002 global data set of the objectively analysed air-sea fluxes (http://oaflux.whoi.edu) data at daily temporal and 1° spatial (linearly interpolated onto 0.25°) resolutions were used. The wind stress, $\tau(\tau_x, \tau_y)$, was obtained from daily global data set at 0.25° resolution. Wind stresses was computed from blended vector sea surface winds (at 10-m above sea level). Details about the wind stress can be obtained at the NOAA website (https://www.ncdc.noaa.gov). The biological model was forced by daily photosynthetically available radiation (I_0, Einstein (E) m^{-2} d^{-1} converted to W m^{-2} as $W = E \times 6 \times 10^{23} \times (86400 \times 2.77 \times 10^{18})^{-1}$) obtained from the GlobColour Project (http://www.globcolour.info/) at a spatial resolution of 0.25°.

3.3.1.5 Numerical Experiment

The numerical experiment was conducted on individual eddy for eddies identified from September 1997 through 2011. Eddies identified in fall or before through spring of the following year were selected for analysis and their tracks are shown in Figure 3.5. Summary of eddies used in the experiment is shown in Table 3.2.

A spin up integration was performed before the simulation on the eddy track and it was initiated in October. This experiment was done using a composite forcing data from 1998 to

2011 repeated over 4 years. From this integration, the last year of simulation was first compared to satellite and *in situ* observations to verify whether the model is reproducing the temporal and vertical pattern of biological fields (CHL) in eddies. The simulated PHY was converted to CHL based on molar ratios above mentioned molar ratios (3.3.1.4). Then, the last year of simulation was used to initialise the model in each experiment. The information of the two example eddies used to study the spring initiation are shown in Table 3.2.

3.3.1.6 Metrics for the Spring Bloom Initiation

The spring bloom initiation can be quantified based on the existing theories of bloom initiation. For verifying the convection shutdown hypothesis (Taylor and Ferrari 2011), a shutdown convection time can be defined as the time when Q_0 switches from winter cooling into spring warming (Ferrari et al. 2015). So, the convection shutdown time was defined as the first day in each calendar year when Q_0 became positive. Following the convection shutdown time, phytoplankton is expected to rapidly increase (Ferrari et al. 2015).

In terms of the underlying mechanisms leading to a spring bloom, the model output provides the necessary information to assess the interacting factors that culminate in a bloom. In addition to the convection shutdown time, we assessed the time change of phytoplankton division (μ) and destruction (l) from the model. The difference between μ and l gives a measure of the net phytoplankton accumulation rate (r_P). A bloom, i.e., accumulation of PHY occurs when $\bar{\mu}$ outweighs $\bar{l}$ and r_P become positive. Thus, from this perspective, the initiation of the bloom is defined as time when the PHY population net growth rate becomes positive ($r_P > 0$). To calculate r_P, μ and $l$were integrated over the TLD or MLD (to obtain $\bar{\mu}$ and $\bar{l}$) whenever TLD was not defined (see the definition of TLD, 3.3.1.1).

$$r_P = \bar{\mu} - \bar{l} \tag{3.14}$$

with

$$\bar{\mu} = \frac{1}{\langle PHY \rangle} \int_z^0 U_P dz \tag{3.15}$$

$$\bar{l} = \frac{1}{\langle PHY \rangle} \int_z^0 (R_P + M_P + G_Z) dz \tag{3.16}$$

$$\langle PHY \rangle = \int_z^0 PHY dz \tag{3.17}$$

where U_P (3.10), R_P (second term in (3.6)), M_P (third term in (3.6)), and G_Z (3.12) are the rates of phytoplankton photosynthesis, of respiration, of mortality, and of mortality due to zooplankton grazing, respectively. Each term of Eq. (3.16) was also separately integrated to obtain $\bar{R}_P$, $\bar{M}_P$, and $\bar{G}_Z$. In addition to these loss terms, nutrient (L_N) and light (L_I) limitations terms were similarly integrated to get $\bar{L}_N$ and $\bar{L}_I$. The above terms were used in section 3.3.4 to investigate their role on PHY dynamics.

The dynamics of the biological components in the model are impacted by the physical turbulence model through diffusion (Eq. (3.5)) and in addition to turbulent mixing within the turbulent layer, the eddy diffusion also accounts for the entrainment and detrainment associated with mixed layer temporal variation, i.e., deepening/shallowing. Thus, we computed the rate of change of TLD (r_{TLD}) to see the covariation with r_P. r_{TLD} was computed in a similar way to the rate of change of PHY as in Boss and Behrenfeld (2010) defined as

$$r_{TLD} = \frac{1}{TLD} \frac{dTLD}{dt} \approx \frac{2(TLD_1 - TLD_0)}{\Delta t (TLD_1 + TLD_0)} \tag{3.18}$$

with $\Delta t = t_1 - t_0 = 1$day. The rate of change of TLD represents the rate of dilution ($r_{TLD} > 0$) and detrainment ($r_{TLD} < 0$) of PHY in the TLD (Mignot et al. 2018).

3.3. Results

3.3.1. Model Verification

Our objective was to understand the influence of eddies on spring bloom initiation based on model simulation. The information available in any specific eddy that could be compared with model results was limited. As there was paucity of *in situ* data within eddies, combining the information in eddies in different years, a mean condition in the interior of eddies could be obtained. From there, the simulation was then performed first based climatological integration for AEs and CEs to verify the ability of the model in reproducing the temporal pattern of phytoplankton seasonal cycle in eddies in the study region. The last year of the climatological integration was compared with *in situ* observations collected within AEs and CEs. In next subsections (3.3.1.1 and 3.3.1.2) we described the comparison between modelled and observed temperature (3.3.1.1) and CHL (3.3.1.2).

3.3.1.1 Temperature

The simulated temperature profiles in the last year of integration were compared with monthly composites of *in situ* data (Figure 3.6). The main features of the vertical structure of temperature were consistent between model results and observations. The seasonal cycle of temperature in CEs and AEs was generally similar. Most of the temperature variation in the model was observed in the upper 100 m (CEs) and 190 m (AEs).

In AEs, surface temperature varied from a minimum in March of about 11ºC to a maximum in August (~25ºC). The main thermocline, where temperature gradient was larger

than 0.02 ºC m^{-1}, was located below 150 m and extended to about 300 m. Above the main thermocline, a seasonal thermocline developed from April to August. In September, surface temperature started to decrease, and the surface stratification was destroyed to form a homogeneous layer of more 150 m in February-March.

In CEs, on the other hand, the permanent thermocline was shallower and extended from nearly 100 m to about 200 m. The minimum of 11ºC was similar to AEs and was observed in February instead of March. Like AEs, the maximum surface temperature in CEs was also observed in August. The mixed-layer appeared to be overestimated in CEs from January to May. As the model is forced by Q_0, the mixed-layer deepens until around mid-March when Q_0 turns positive. We observed that within a given month, the model variation in temperature was smaller than in the observations and in the deep layers there was almost no variation. It is expected that the model was mainly showing only the seasonal evolution of the temperature while the observations included the spatial and temporal variability in the eddy areas which can be much different in the centre than near the edge. So, with these factors in mind, the temporal variation of the vertical structure of observed temperature was reasonably well captured by the model.

3.3.1.2 CHL concentration

The modelled distribution of PHY in the last year of simulation was first converted to CHL and then compared with the 10-year composites of satellite CHL (Figure 3.7). The main features of the seasonal cycle of ecosystem dynamics in the mesoscale eddies of the Japan Sea were remarkably well reproduced in the model. The annual cycle of phytoplankton was characterised by a pronounced spring bloom and a weak autumn bloom (Figure 3.7). CHL was low in winter (January-February) in both AEs and CEs and increased at the end of January and beginning of March in CEs and AEs, respectively. In mid-March, CHL was

more than 1 mg m^{-3} in CEs, whereas the same concentration level was reached in April in AEs. The spring bloom, CHL > 1 mg m^{-3}, was observed in April in both eddy types. After the spring bloom, summer conditions were dominated by low concentrations (CHL < 0.3 mg m^{-3}). From September, CHL increased gradually from less 0.3 mg m^{-3} to about 0.6 and 0.7 mg m^{-3} in November in AEs and CEs, respectively, and declined thereafter.

The vertical profiles of CHL also showed that in winter (January-February) CHL was low (< 0.5 mg m^{-3}) in AEs. But it was slightly higher in CEs. Moreover, CHL was homogeneously distributed within the mixed layer, especially in January in AEs. During summer, the surface concentration was lower than during winter (Figure 3.8). In April, the observations did not show the spring bloom with CHL > 1 mg m^{-3} at the surface in AEs, as seen in the satellite data. This could be related with the sampling period of *in situ* data. After the spring bloom peak, a subsurface CHL maximum developed during the stratified periods. The subsurface maximum gradually moved downward and decreased from around 40 m and ~0.8 mg m^{-3} in May to nearly 60 m and ~0.6 mg m^{-3} in July, respectively in both AEs and CEs. From October the nearly homogeneous vertical distribution was again developed in the upper mixed-layer. Overall, the model consistently resolved well the temporal variations of the vertical conditions of CHL observed in both AEs and CEs.

3.3.2. Experiments along Eddy Tracks

The above results demonstrated based on the climatological integration demonstrated the ability of the model in capturing the main features of the ecosystem dynamics associated with eddies in the study area. Therefore, in this section, we looked at an individual eddy and detailed the dynamics of PHY associated. The last year of the climatological simulation was used as initial condition for the experiments along the eddy tracks. From the model, the temporal evolution of different parameters (e.g., MLD) was compared with the temporal variability of PHY (CHL) to evaluate the spring bloom initiation following an individual

eddy in the study region (Figure 3.5, Table 3.2). In this part, we introduce two examples of the experiments along eddy tracks, one for AEs and the other for CEs.

We start with the description of the conditions over the track of an AE (A249) initially identified on 20th September 2000 tracked through 11th December 2001 totalling 64 weeks of lifespan. The characteristics of the seasonal cycle of the physical and biological fields (Figure 3.9) along the eddy tracks are described below.

MLD increased steadily to about 50 m from October to November. It then deepened rapidly from November to January. Maximum MLD (~200 m) was observed in March. The transition between deep MLD in winter to shallow spring-summer MLD was abrupt in A249. The MLD rapidly shoaled within a month from about 200 m in March to less than 50 m in April. During the deepening of the MLD, DIN was replenished in the surface layers and the concentration was higher (> 4 mmol N m^{-3}) as compared to the stratified period (DIN $\ll$ 4 mmol N m^{-3}) (Figure 3.9c-d).

PHY was low during the shallow MLD period (Figure 3.9a) and initially increased slightly with MLD deepening. Further increase in the MLD decreased PHY and it became lower than 0.2 mmol N m^{-3}, meanwhile I_0 decreased (Figure 3.9i) and DIN was increased (Figure 3.9c). The lowest I_0 was in early January, and it increased thereafter. Beginning of March, PHY started to increase while the MLD was deep. Later with the reduction in the depth of turbulent mixing (TLD), PHY increased rapidly and bloomed (>0.8 mmol N m^{-3}) at shallow depths in the range of Z_{eu} (Figure 3.9a). During the blooming, DIN and I_0 were high in the surface (Figure 3.9b, c and i) and subsequently DIN decreased while I_0 continued to increase (Figure 3.9i).

A subsurface PHY maximum was formed at the base of seasonal nutricline from the end of April when the surface concentration was declining. This subsurface maximum

deepened from about 30 m at the end of April to nearly 60 m in July. The concentration of ZOO (Figure 3.9e) and DET (Figure 3.9g) increased considerably in spring when PHY concentration was also high. DET compartment represents dead PHY and ZOO and large fraction of dead organic material that sinks out of the Z_{eu} was observed in April (Figure 3.9g).

Cyclonic eddy (C325) was identified on 14th August 2002 and tracked through 24th June 2003 with a span of about 45 weeks. In C325, similar to A249, DIN was high during the deep MLD (Figure 3.9d). In November, autumn bloom (PHY >0.4 mmol N m^{-3}, Figure 3.9b) developed in C325 when the MLD deepened and DIN increased in contrast to A249 where the autumn bloom was absent (PHY $\ll$0.4 mmol N m^{-3}, Figure 3.9a). The deepest MLD (~117 m) in C325 was observed in February, and it was not much different from the Z_{eu} (max. difference of ~60 m during the deepest MLD). In contrast, the difference was more than 100 m in A249.

The blooming of PHY was earlier in C325 as high PHY (>0.4 mmol N m^{-3}) was initially observed in the end of February over the whole depth of TLD (Figure 3.9b). It was slightly diminished and remained ~0.4 mmol N m^{-3} with the increase in TLD, but rapidly increased again when TLD ~ Z_{eu} in mid-March. After the blooming, the subsurface maximum was formed initially at shallower depth (~20 m) in April and then deepened to about a similar depth as in A249 of 60 m in the end of May.

The concentration of PHY, and also that of ZOO (Figure 3.9f) and DET (Figure 3.9h), was relatively higher in C325 as compared to A249 from autumn to spring except in December when the lowest PHY and I_0 were observed in C325 (Figure 3.9a and b). Although the MLD was shallower in C325 than in A249, the winter levels of DIN in both A249 and C325 were almost in a similar range (~ 5-6 mmol N m^{-3}). The main nutricline (>0.2 mmol N m^{-4}) was shallower (~100 m) in C325 and deeper in A249, >150 m.

3.3.3. Convective Mixing and Bloom Initiation

Convective mixing began in October when Q_0 turned negative in A249 (Figure 3.10e). Q_0 remained negative from October until mid-March when it switched to positive in early spring (Figure 3.10c). During the cooling period, eddy diffusivity (κ) was increased $>10^{-2}$ m^2 s^{-1} and remained high while the heat loss was large. The MLD (TLD) during $Q_0 < 0$ and $\kappa > 10^{-2}$ m^2 s^{-1} deepened to about 200 m (~175 m) in mid-March. The TLD then rapidly decreased following the switch of Q_0 to positive. Meanwhile, the MLD remained deep. A subsequent cooling event associated with Q_0 fluctuations at the end of March resulted in transient increase in κ and thus deepened both the TLD and MLD. As Q_0 continued to increase, the MLD also shallowed rapidly. From April, when $Q_0 > 0$, TLD was not defined as κ significantly decreased and became $<10^{-2}$ m^2 s^{-1}.

CHL barely increased in A249 when the MLD started deepening in October and the autumn bloom was absent (CHL < 1 mg m^{-3}, Figure 3.10a). Winter conditions were dominated by low CHL concentration, generally lower than 0.5 mg m^{-3} between January and March. I_0 was low in winter and started increasing in January (Figure 3.10c). The minimum of surface CHL corresponded to the minimum of I_0 observed in January. During this time, PHY was being circulated over deep turbulent convective layer (TLD > 100 m). After that, CHL increased slowly along with the increase in I_0 (Figure 3.10a and c). The spring bloom associated with the exponential increase in CHL concentration was initiated at the shutdown time of the convection when Q_0 turned positive and TLD decreased significantly while MLD was deep (~200 m).

Fluctuations of Q_0 at the end of March caused transient decline in CHL as PHY was again mixed to relatively deep layers (Figure 3.10a). However, for fluctuations of $\kappa < 10^{-2}$ m^2 s^{-1}, the effect on MLD variation was negligible and thus the concentration of CHL was not

impacted. For example, the spring bloom peak (~4 mg m^{-3}) in A249 was delayed, when κ increased (>10^{-2} m^2 s^{-1}) and was observed in the first half of April after further decrease in κ and rapid shallowing of MLD (Figure 3.10a).

In the CE, in less than a month, Q_0 decreased rapidly from more than –100 W m^{-2} to about –500 W m^{-2} (Figure 3.10f). MLD (TLD) and κ also increased rapidly (Figure 3.10d). From November to February, Q_0 fluctuated within the range from –500 to –200 W m^{-2}. During that time, κ was nearly constant and MLD (TLD) was deepening steadily. In February when heat loss decreased to ~ –100 W m^{-2}, the MLD changed slightly from ~117 to 100 m, whereas the TLD decreased from ~100 m to <80 m. In C325 where MLD was shallow, turbulent mixing was limited to shallow depths almost in the range of the Z_{eu}. The TLD became shallower than Z_{eu} while $Q_0 < 0$. Similarly, MLD also started shallowing during negative Q_0 and around the second half of March when net cooling subsided, MLD was already shallower than Z_{eu},

CHL, in the CE, was always >0.5 mg m–3 except in December when minimum I0 was observed (Figure 3.10b). The first increase in CHL of ~1 mg m–3 preceded the end of winter cooling. This rapid increase in CHL was initiated in February and fluctuated at the beginning of March when Q0 decreased. After that, CHL was ~2 mg m–3 in C325 when Q0 turned positive. So, convective mixing did not appear to control this initial increase in CHL associated with the spring bloom in C325. As seen in satellite data, CHL was at peak concentrations at the shutdown convection time. The magnitude of spring bloom peak in C325 was relatively earlier and higher than in A249.

3.3.4. Rate of Net Phytoplankton Accumulation and Ecosystem Dynamics

We evaluated the role of the key variables in the model playing a role in the variability of PHY. As mentioned in previous sections, at the beginning of the cooling season, around

September-October, increased turbulence in the mixed-layer deepened the MLD. As a resulted, DIN stocks were replenished due to entrainment ($r_{TLD} > 0$). Thus, nutrient limitation ($\bar{L}_N$) was lifted in both A249 and C325 (Figure 3.11). The increase in the depth of turbulent mixing resulted in reduced light levels ($\bar{L}_I$) within this layer (Figure 3.11c-d).

In A249, the lowest surface PHY (hereafter SPHY, Figure 3.11e) concentration (~0.1 mmol N m^{-3}) followed the lowest $\bar{L}_I$ observed in January Figure 3.11e). Before and after that time, SPHY varied consistently with $\bar{L}_I$ and developed a SPHY bloom in March when net cooling subsided and both light and nutrients were high. After the spring bloom peak of >2 mmol N m^{-3} in April, SPHY declined due to combined effects of nutrient depletion and increase in ZOO grazing ($\bar{G}_Z$, Figure 3.11c).

The net phytoplankton accumulation rate (r_P) indicates the interactions between community division ($\bar{\mu}$) and loss ($\bar{l}$) rates. For a bloom r_P should be positive. The positive r_P, i.e., the accumulation or growth phase of PHY, was observed from autumn when turbulent mixing was developing and TLD was deepening ($r_{TLD} > 0$, Figure 3.11a). It remained positive almost throughout the autumn to spring with accumulation rates <0.1 d^{-1}. In March-April when net cooling subsided, r_P increased considerably, >0.2 d^{-1}. This later and rapid increase in r_P was associated with the bloom initiation in A249. Thus, to make a distinction between the winter and spring positive growth phases, the initiation of the spring bloom will be referred to the period of exponential increase observed in March.

During the winter growth phase in A249, the integrated PHY (ΣPHY) developed unchecked by ZOO grazing, which had significantly decreased in January (Figure 3.11c) when the effect of dilution due to entrainment had ceased ($r_{TLD} \sim 0$). The first bloom peak of ΣPHY of ~60 mmol N m^{-2} was at the beginning of March just before the end of net cooling and rapid shoaling of TLD ($r_{TLD} < 0$). The spring bloom peak of ΣPHY (~75 mmol N m^{-2})

followed at the end of March (Figure 3.11e) after the large r_{TLD} fluctuation. The ΣZOO levels remained almost constant after the initial increase until around the end of February. After March, ΣZOO then varied in response to food availability as they feed on PHY. The spring bloom is typically associated with decrease in MLD or TLD and rapid accumulation of PHY. The two large and negative r_{TLD} in March-April were concomitant with the large r_P >0.2 d^{-1}. So, this rapid change of r_{TLD} in mid-March contributed to the large increase in r_P which marked the initiation of the spring bloom with strong surface signature.

In C325, the temporal variation of SPHY and ΣPHY was somewhat similar, particularly in winter (Figure 3.11f). Contrary to A249, in October $\bar{L}_N$ rapidly increased to >0.5 d^{-1} within a month in C325 while light levels where still relatively high. This caused a noticeable increase in SPHY in November, in response to DIN supply. Mean SPHY in C325 was lowest (~0.12 mmol N m^{-3}) in December after the minimum $\bar{L}_I$. Thereafter, SPHY varied consistently with $\bar{L}_I$ and generally increased until the spring bloom peak (>2 mmol N m^{-3}) in the second half of March. While the blooming PHY quickly exhausted DIN, additional input of DIN into the mixed-layer in the beginning of April caused a second PHY peak around mid-April. The second peak was lower than the first as $\bar{G}_Z$ had already increased and could keep pace of the increasing food availability (Figure 3.11b).

The time series of r_P in C325 indicated several autumn-winter growth periods with larger accumulation rates (>0.1 d^{-1}) than in A249 (Figure 3.11a, b). In C325 where the MLD was shallow, the effects of dilution were small and ZOO grazing could always feed on PHY whenever food became available. In fact, variation of ΣZOO closely followed the increases in ΣPHY (Figure 3.11f). We note that in C325, several exponential increases in r_P with relatively significant surface expression of PHY were observed during winter.

Similar to A249, the spring accumulation phase in C325 was much larger than the winter, and it was also associated with the rapid decrease in r_{TLD}. However, in C325, the first large r_P ($> 0.2\ \mathrm{d}^{-1}$) was not associated with the shutdown of convection as it occurred much earlier while $Q_0 < 0$. This means that in CE, PHY blooms may represent a continuous growth period from autumn to spring that culminates in larger r_P in spring when growth conditions are optimal.

It is worth noting that in winter the negative r_P in C325 was mostly caused by grazing due to ZOO, whereas in A249 it was associated with the decline in light. In A249, for instance, the lowest $\bar{l}$ was observed in January and community respiration ($\bar{R}_P$) at that time corresponded to ~50% of $\bar{l}$. This showed that, although losses due to ZOO grazing were very low (Figure 3.11c), light limitation was severe enough so that $\bar{R}_P$ was >60% of $\bar{\mu}$ and thus $r_P < 0$.

3.4. Discussion

We studied the spring bloom initiation associated with mesoscale AEs and CEs based on 1D coupled physical-biological model. The two examples provided an understanding of the differences in ecosystem dynamics between AEs and CEs during the spring bloom initiation. Both biotic and abiotic processes have been known to play a key role in initiating the spring bloom (e.g., Sverdrup 1953). Therefore, initiation timing of the spring bloom estimated based on net PHY accumulation rate was compared with the time when net cooling subsided. By looking at the time when convection shutdown, we were interested in understanding the relation between the end of winter cooling and the associated suppression of turbulent convective mixing with the initiation of the spring bloom in AEs and CEs.

3.4.1. Limitations of 1D Modelling

Our modelling approach successfully resolved the variability of the ecosystem associated with AEs and CEs. A good agreement was found between two independent validation datasets namely *in situ* and satellite observation. Thus, the model provided a good means for the study of bloom initiation in AEs and CEs. Nevertheless, given the assumptions taken in the model's formulation and the limitations inherent to these assumptions, some aspects worth of further study are discussing below.

The 1D model is unable to simulate the typical 3D oceanic environment. It is known that 3D oceanic processes may play a role in initiating a bloom (Mahadevan et al. 2012). In our modelling, we introduced the restoration term to compensate for some of these 3D features, such as horizontal advection. In certain regions of the global ocean, such as the subtropical gyres, the mesoscale horizontal transport of nutrient is known to predominate over the vertical nutrient supply (Garçon et al. 2001). In our model, during summer, when vertical diffusion dropped considerably, phytoplankton became nutrient limited and the restoration supplied some nutrient to maintain reasonable background concentrations of CHL. However, this restoration had no effect on the results obtained during nutrient-replete period, prior to stratification, which was central to the current study. During the stratified period in summer, oligotrophic conditions prevail, and horizontal nutrient supply may be of relevant importance in this area as well, although further research should clarify this issue.

3.4.2. Convective Mixing

The convection shutdown hypothesis predicts a bloom to initiate when turbulent mixing weakens at the end of winter, thereby causing PHY to increase rapidly in a bloom (Taylor and Ferrari 2011; Ferrari et al. 2015). In the case of the AE analysed results were consistent with the above hypothesis. Deep MLD developed during winter cooling and the MLD generally corresponded to the TLD. In spring, when net cooling subsided, TLD shoaled

rapidly while MLD remained deep. CHL then began increasing rapidly in the shallowing TLD (Figure 3.10c). Moreover, the result also supports the speculation made by Maúre et al. (2017) that in AEs blooms are initiated by the weakening of convective mixing. Therefore, our modelling experiment confirmed that suppression of turbulent mixing plays an important role in initiating the blooms in AEs.

In the case of the CEs with shallow mixed-layers, Maúre et al. (2017) suggested that the spring bloom was initiated by increase in mixed-layer average light (I_{ML} ~5.6 E m^{-2} d^{-1}) while the turbulent mixing is strong ($Q_0 \ll 0$). Based on the 1D model, we found support for this observation. The rapid increase in CHL was initiated in February when TLD decreased to ~80 m while Q_0 was negative (Figure 3.10d, f). We estimated the TLD mean light from the model in February and found that it increased from ~2.4 to ~4.0 E m^{-2} d^{-1} slightly lower than the above mentioned value. I_0 also increased rapidly in February from ~13 to 24 E m^{-2} d^{-1} when CHL initiated the rapid increase. It is worth noting that the TLD was slightly deeper than Maúre et al's MLD and that in this study MLD and TLD were not significantly different in CEs in the whole time series. This indicates that increase in I_0 in the shallow TLD increases the mean light conditions and triggers earlier blooms while turbulent mixing is strong.

In different oceanic regions, increased light levels within the mixed layer, have also been found to initiate the spring blooms (Siegel et al. 2002; Venables and Moore 2010; Itoh et al. 2015) and in some instances even prior to the end of net cooling (Mahadevan et al. 2012). In the Southern Ocean, Venables and Moore (2010) investigated the potential of light limitation for phytoplankton growth. Using areas near islands where mixed-layers are shallow and iron limitation has been lifted, they found significant increase in CHL for I_{ML} >3.0 E m^{-2} d^{-1}. Itoh et al. (2015) used profiling float observations with biological sensors in the Kuroshio–Oyashio Extension region and found a significant CHL response to increase in the

I_{ML} for values typically >4.0 E m^{-2} d^{-1}, corresponding to I_0 >20 E m^{-2} d^{-1}. These observation clearly support the idea that for shallow mixed-layers (Hitchcock and Smayda 1977), bloom are triggered by the improved light conditions even prior to the end of net cooling.

Brody and Lozier (2014) also suggested that blooms initiate when negative heat fluxes weaken and shift the mixing mechanism from convection to wind driven. These conditions may be close to AEs, κ decreasing and TLD shoaling. In CEs, the depth range of TLD plays an important role in modulating the light conditions for PHY and in initiating the blooms. For example, in February, enhanced CHL (Figure 3.10b), was observed when TLD decreased while the mixing conditions was still largely convective ($\kappa > 10^{-2}$ m^2 s^{-1}). Therefore, in CEs even if the mixing mechanism is still dominated by convection, blooms advance prior to the shutdown of convective mixing (Maúre et al. 2017) or to the switch in the mixing length scale (Brody and Lozier 2014), because of the shallow TLD.

3.4.3. Grazing Influence

The disturbance-recovery hypothesis proposed by Behrenfeld et al. (2013a) suggests that the growth phase of PHY is initiated in winter largely by the physical disturbance of PHY-ZOO interactions during the MLD deepening. This disturbance is suggested to have a strong impact on grazing because of the decrease in encounter rates caused by dilutions effects. ∑PHY then starts increasing because of the large decrease in grazing even though PHY division rates also decrease with decreasing light and deepening MLD (Behrenfeld 2010; Behrenfeld et al. 2013a). Based on the net PHY accumulation rate, we found that PHY growth in the AE started in winter and this was consistent with other studies (Boss and Behrenfeld 2010; Behrenfeld 2010; Behrenfeld et al. 2013a; Mignot et al. 2018; Yoshie et al. 2003)

The above mechanism provides considerations for the winter increase in ΣPHY, but it does not provide an explanation for the initiation of blooms in surface (Chiswell et al. 2015). This may partly be related with the fact that Behrenfeld et al. (2013a) found little response in r_P to the large springtime increases in $\bar{\mu}$. Our modelling results showed large values of r_P in spring for both AE and CE. Therefore, the results from this modelling indicated that although the growth phase started in winter while the MLD was deepening in the AE, the initiation of the spring blooms followed in spring with the exponential growth (Mignot et al. 2018).

In the CE, MLD was shallow and the dilution effect was also smaller. Therefore, no significant disturbance of the grazing by the deepening of the MLD was expected (Behrenfeld et al. 2013a; Marra et al. 2015). In fact, the interactions between PHY and ZOO were quite tight (Figure 3.11f) and their concentration was higher than in AE in almost the entire time series. Several and larger net accumulation phases (r_P > 0.1 d^{-1}) were observed throughout the autumn-spring period with considerable surface expression than in AE. As the coupling PHY and ZOO was barely disrupted in the CE, even during the rapid accumulation rate observed in beginning of March, the maximum of ΣPHY was lower (<70 mmol N m^{-2}) than in the AE because grazing could keep pace of the food availability (Figure 3.11e-f). So in CEs, the conditions controlling the PHY division play a crucial role for the initiation of blooms as we suggested above.

Mignot et al. (2018) studied the North Atlantic bloom based on bio-optical floats. They discussed the potential role of weak winter accumulation phase and the possibility of being a precursor of the spring bloom. They also suggested that the winter accumulation phase requires deep mixed-layers so that regions with weaker dilution effects are expected to have no winter accumulation. Our observations of winter accumulation phase in the AE support their speculations about the deep mixed-layer and weak winter accumulation phase. In the CE with weak dilution, we found relatively stronger winter accumulation phase because $\bar{L}_I$ was

relatively higher and allowed for sporadic and fast accumulation phases. This means that in shallow mixed-layers, although the grazing counters the rapid growth, improved light exposure will play an important role in triggering a rapid r_P even during winter (Figure 3.11d).

Our model only included a single PHY component and the assessment of the winter accumulation phase being precursor of the spring bloom is difficult without the knowledge of PHY population. However, the winter accumulation rate and concentration of PHY in the CE was larger than in the AE. Then, when r_P increased >0.2 d^{-1} in March, SPHY developed rapidly and peaked, whereas in the AE the peak time was delayed until April. This suggested that the high winter concentration in the CE allows for the rapid peak of PHY during the spring blooms in CEs. In contrast, the weaker winter accumulation and low concentration of PHY delays the spring bloom peak in AES.

Lévy (2015) used a set of numerical experiments to test a number of assumptions associated with the Sverdrup model of spring bloom initiation (Sverdrup 1953) and found that the incorporation of grazing was not sufficient to conform to the dilution-recoupling hypothesis. Kuhn et al. (2015) used an optimised one dimensional NPZD model to assess the assumptions inherent to both the critical depth and the dilution-recoupling hypotheses. Through the analysis of climatological annual cycles of satellite-based PHY biomass in the subpolar North Atlantic, they found support for both bottom-up and top-down hypotheses although neither of their bloom initiation mechanisms fully applied in their experiments.

In our experiment, we found that integrated biomass started increasing in winter in AE, and this is consistent with the dilution-recoupling hypothesis. However, the spring bloom was initiated in March when the net population growth increased exponentially culminating in a pronounced bloom for both SPHY and ∑PHY after the end of cooling in AE. In CE, it appears that winter growth was stronger and modulated by light availability. Increasing light

intensity allowed for high light exposure and bloom initiation prior to the end of net cooling. Overall, modelled ZOO strongly controlled PHY biomass in CE. As grazing has a lagged response to food availability, whenever PHY growth conditions were permitting, PHY increased rapidly before ZOO could catch up. In the AE, recoupling between PHY-ZOO was only observed after the spring bloom peak ∑PHY.

3.5. Conclusions

In this study, a coupled turbulence physical-biological model was applied for the study of spring bloom initiation associated with mesoscale AEs and CEs. By running a set of two separate experiments, one in AEs and the other in CEs, we were able to reproduce the dynamics of the mixed-layer associated with eddies and the associated biological dynamics. The NPZD model used was able to reproduce well the dynamics of chlorophyll-a in mesoscale eddies evidenced by the good agreement with observations (both *in situ* and satellite) and thus demonstrated the role played by mesoscale eddies in the temporal variability of bloom initiation.

Our results first confirmed the speculations based on surface heat flux data that in AEs blooms are delayed due to strong turbulent mixing and are initiated when the depth of turbulent mixing decreases before the stratification of the MLD. The model resolved the temporal and vertical variations of eddy diffusivity (κ), and thus we clearly showed that blooms, indeed, are triggered by the weakening of turbulent mixing in AEs. Therefore our modelling supports the conclusions of Maúre et al. (2017). In the CEs, we also confirmed that early blooms advance in the presence of strong mixing. The shallow mixed-layer allowed for the average light conditions in the TLD (or MLD) to be improved earlier in CEs, thereby triggering the bloom prior to the end of cooling.

Moreover, it was also shown that decrease in grazing rates initiate the growth phase in winter in AE although weaker than the spring exponential growth. In the CEs, winter growth phase was stronger than in AEs. Overall, the model showed that the initiation of blooms strongly depends on mixing conditions in both AEs and CEs which modulates the light availability within the TLD. The termination of the blooms can be linked to increased grazing and nutrient depletion due to strong stratification.

Table 3.1. Definitions, values and units of the parameter used in the ecosystem model

Parameter	Definition	Value	Units
PHYTOPLANKTON TERMS			
$\mu_{\max}$	Maximum photosynthetic rate at 0°C	6.944×10^{-6}	s^{-1}
R_P	Respiration rate at 0°C	3.472×10^{-7}	$°C^{-1}$
M_P	Mortality rate at 0°C	4.629×10^{-7}	$m^3(mmolN\ s)^{-1}$
k_T	Temperature coefficient	0.0693	$°C^{-1}$
k_N	Half saturation constant for N	1.5	$mmolN\ m^{-3}$
k_R	Temperature coefficient for respiration	0.0519	$°C^{-1}$
w_P	Sinking speed of phytoplankton	5.787×10^{-6}[b]	$m\ s^{-1}$
ZOOPLANKTON TERMS			
$g_{\max}$	Maximum grazing rate at 0°C	2.894×10^{-6}	s^{-1}
λ	Ivlev constant	1.620×10^{-5}	$m^3(mmolN\ s)^{-1}$
σ	Threshold value for grazing	0.0745[a] (0.043)	$mmolN\ m^{-3}$
M_Z	Mortality rate at 0°C	8.102×10^{-7}	$m^3(mmolN\ s)^{-1}$
α_Z	Assimilation efficiency	0.7	Dimensionless
β_Z	Growth efficiency	0.3	Dimensionless
DETRITUS TERMS			
r_{DN}	Decomposition rate at 0°C	5.7870×10^{-7}	s^{-1}
w_D	Sinking speed of detritus	5.7870×10^{-5}	$m\ s^{-1}$
OTHER TERMS			
k_W	Light dissipation coefficient of seawater	0.05	m^{-1}
k_P	Self-shading coefficient	0.04	$m^2 mmolN^{-1}$
k_D	Light attenuation by detritus	0.01	$m^2 mmolN^{-1}$

I_{opt}	Optimum light intensity	60[a] (70)	$\mathrm{W\ m^{-2}}$
$\mathrm{C{:}\,CHL}$	Carbon to chlorophyll ratio	50	Dimensionless
$\mathrm{C{:}\,N}$	Carbon to nitrogen ratio	6.625	Dimensionless

a The value was modified from the one in parenthesis to best represents the observations.

b Source: Kuhn et al. (2015)

Table 3.2. List of eddies used to study the spring initiation. The forcing data for the NPZD model were averaged along their tracks.

Eddy ID	Date		Lifetime [Weeks]
	Start	End	
A249	20-Sep-2000	11-Dec-2001	64
C325	14-Aug-2002	24-Jun-2003	45

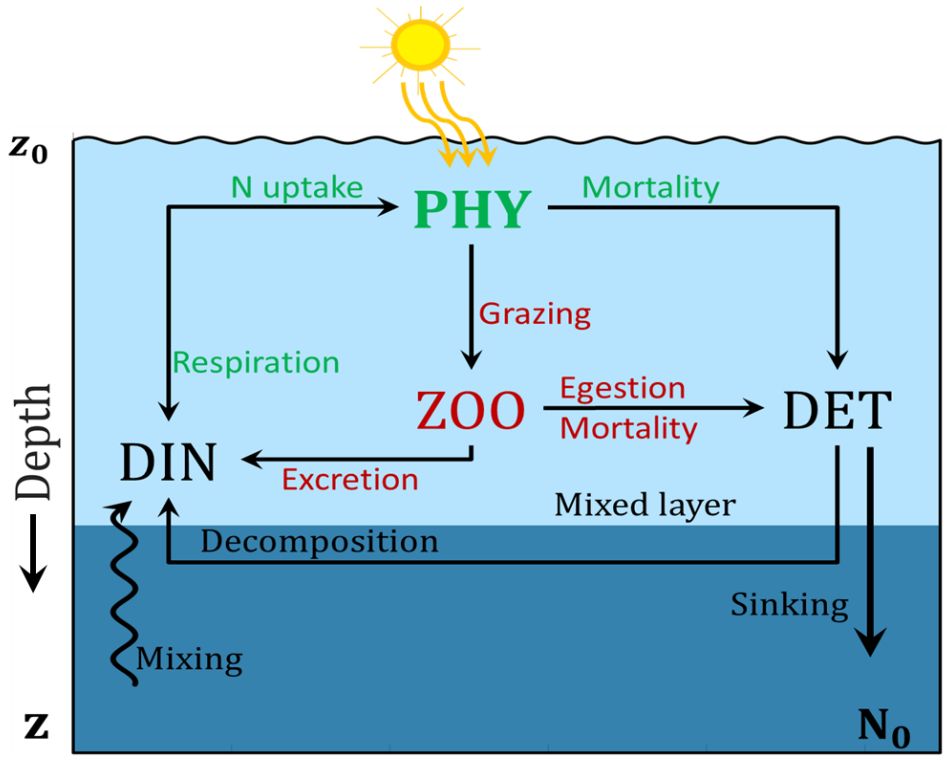

Figure 3.1. Schematic of the Ecosystem model and the processes simulated. N_0 represents the nutrient pool beyond the mixed layer which separates the surface from the deep layers. A detailed description of the processes shown can be found in the text.

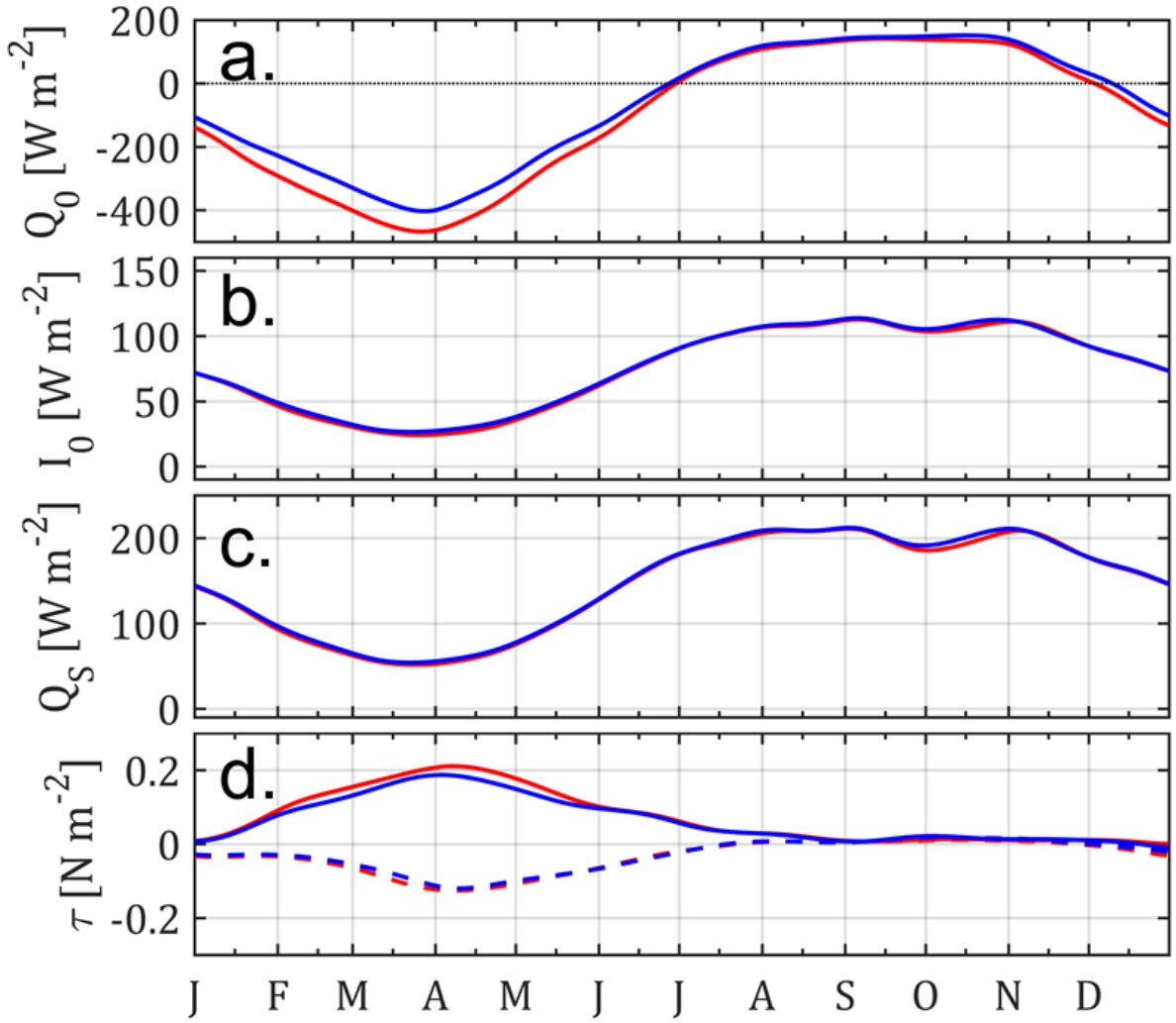

Figure 3.2. Annual cycle of composite (a) net heat flux (Q_0), (b) photosynthetically available radiation at the surface (I_0), (c) shortwave radiation (Q_S) and (d) wind stress (τ) wind solid lines forτ_x and dashed lines for τ_y in AEs (red) and CEs (blue). Over the annual cycle, the areas of negative Q_0 is larger than the positive one. Thus, the annual mean of Q_0 is negative.

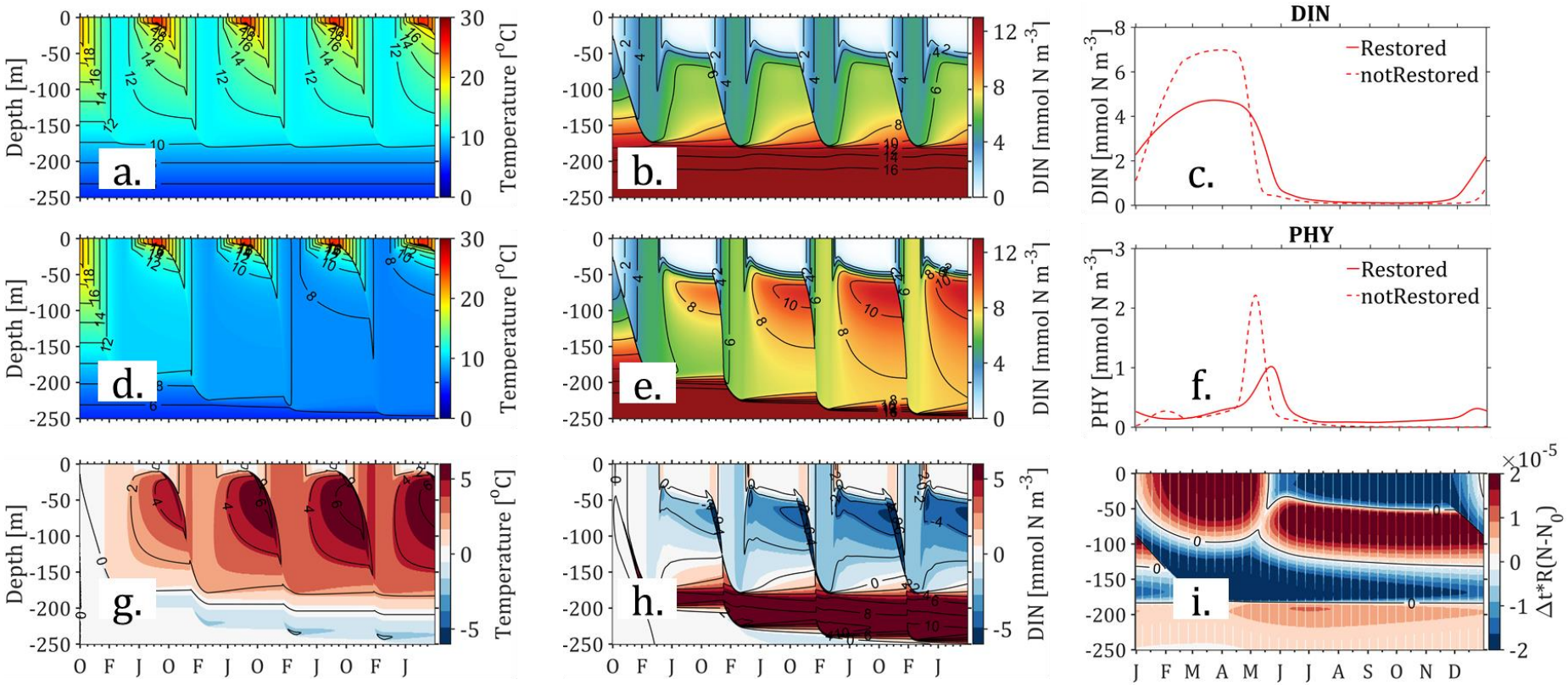

Figure 3.3. Time series of vertical distributions of (a and d) temperature and (b and e) DIN over the 4-year spin up integration and time. series of surface (c) DIN and (f) PHYin the last year of the spin-up integration. In (a-b) are the time series with restoration term applied and (d-e) without restoration term applied. The corresponding surface time series with and without restoration for DIN and PHY and shown in (c and f). Panels (g-h) are the differences between (a, d) and (b, e). The amount of DIN restored in the model—Eq.(3.13)—is shown in (i) in units of DIN.

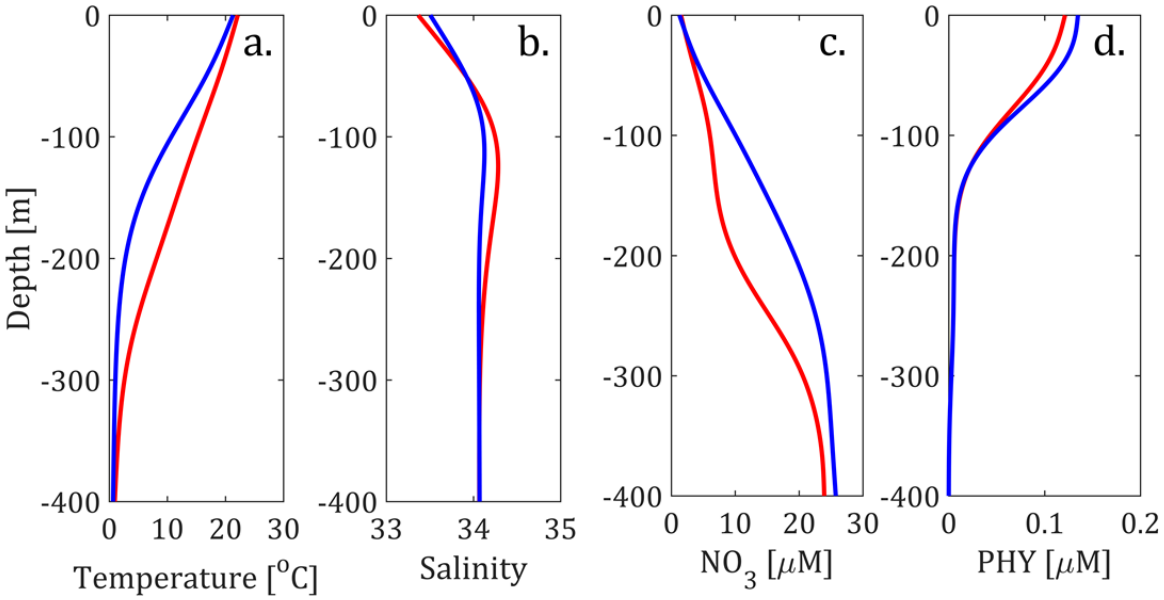

Figure 3.4. Profiles of monthly averages of (a) temperature, (b) salinity, (c) nitrate (DIN) and phytoplankton (PHY) carbon (from CHL) in October. Red and blue indicate profiles in AEs and CEs, respectively. The profiles are originally available at discrete depths with varying resolution. Thus, they were first interpolated onto a uniform grid interval of 1 m in conformity with model resolution and then smoothed with a running mean.

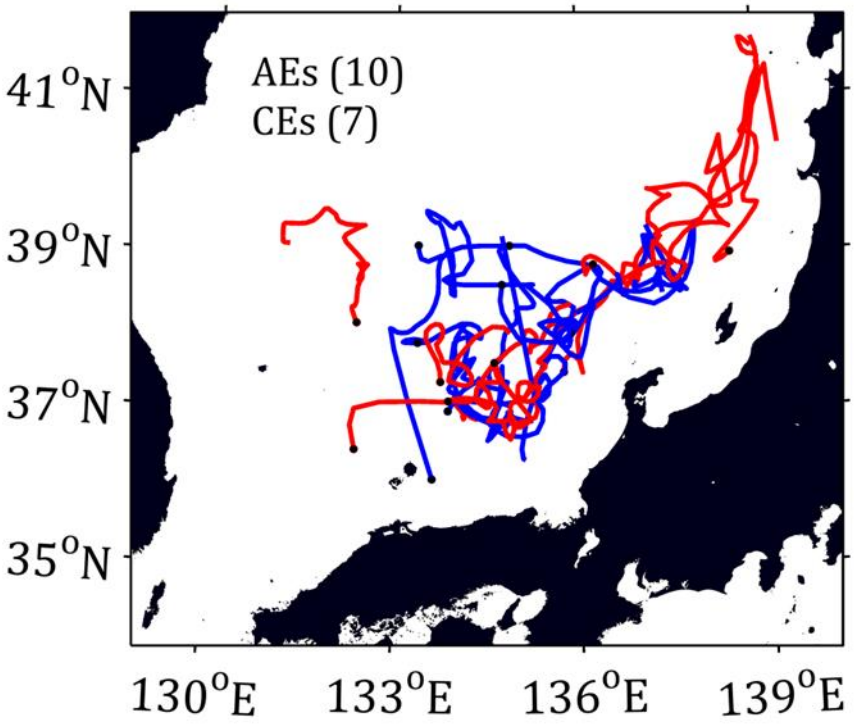

Figure 3.5. Tracks of eddies used in the simulation. Blue and red denote CEs and AEs, respectively. The surface forcing, i.e., Q0, I0, etc., were obtained over each eddy track. Eddies in this panel are those initially identified in the winter or before of the year preceding springtime.

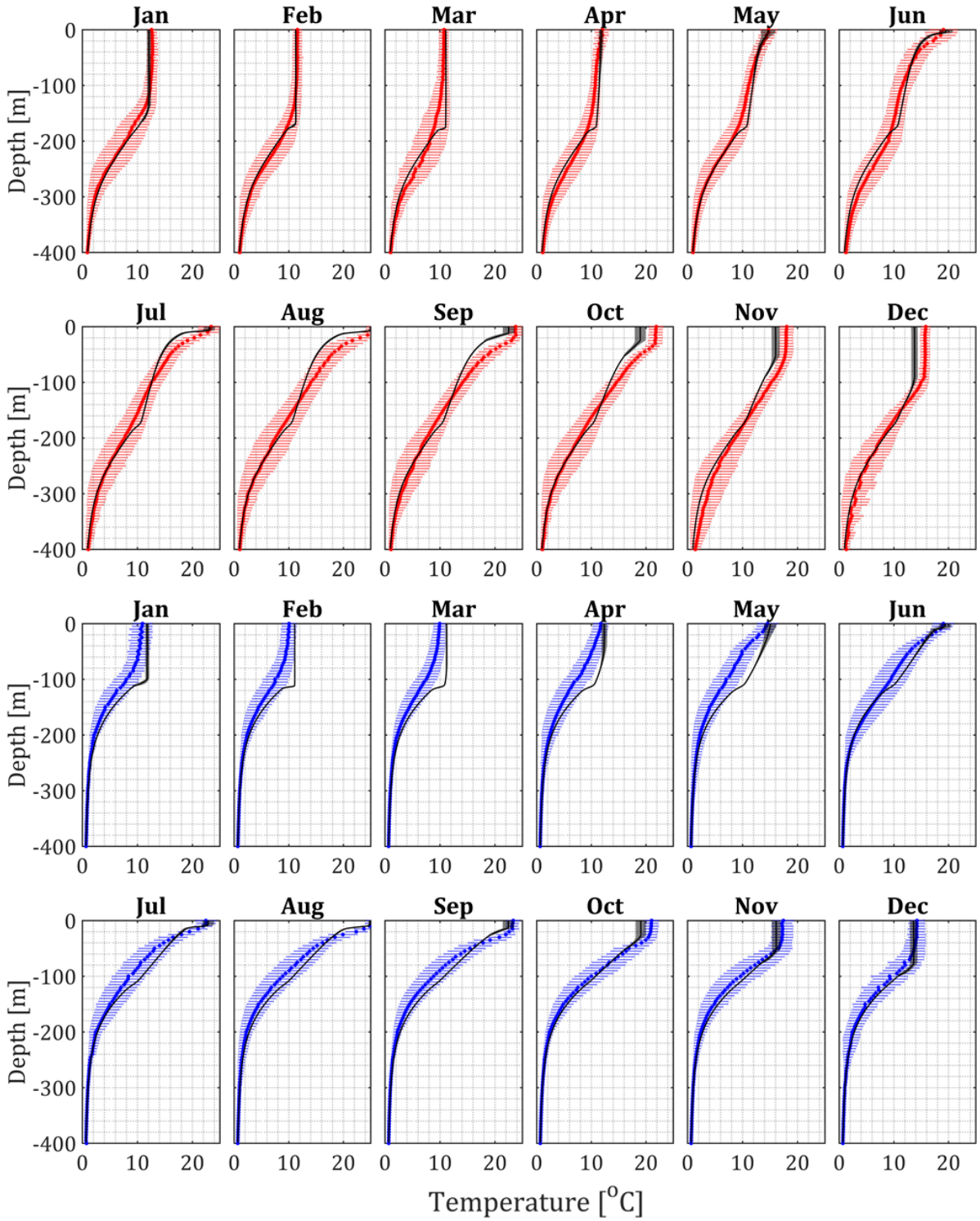

Figure 3.6. Monthly mean distributions of vertical profiles of simulated (black lines) and observed (filled circles) temperature in AEs (red) and CEs (blue) from January to December. Horizontal bars indicate the standard deviation of observations. Shading in the lines indicates the standard deviation on the simulated monthly mean. Note that variation in the model

within a given month was always smaller than in the observations and was mainly in the surface mixed-layer.

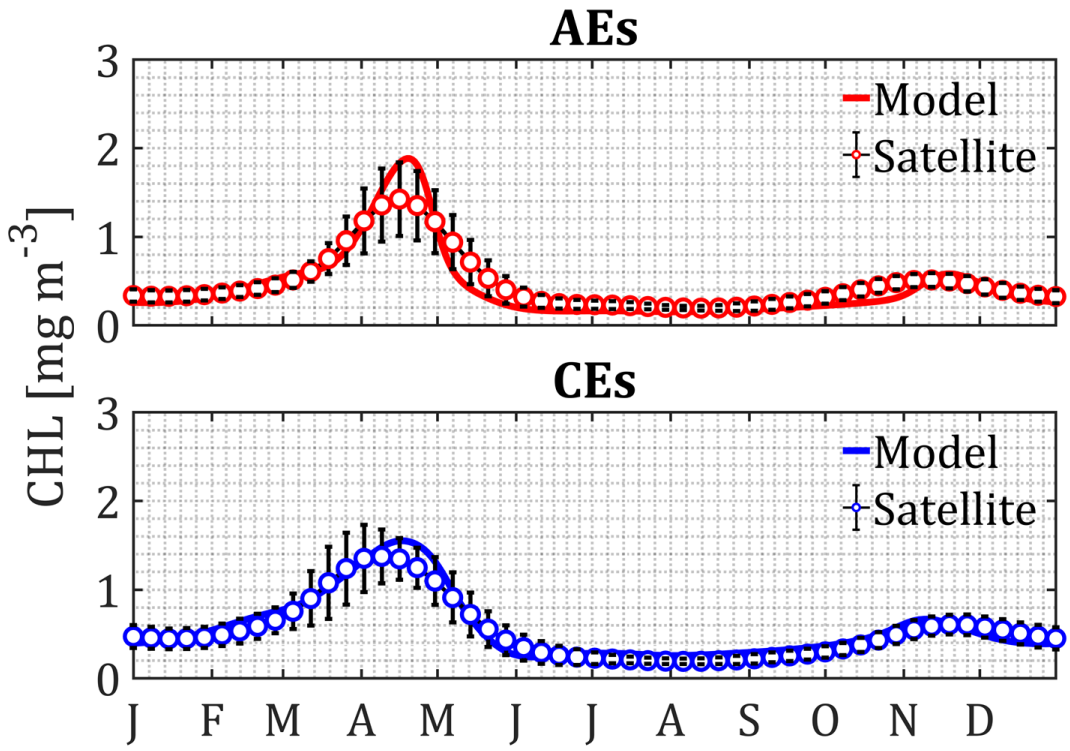

Figure 3.7. Model simulated (lines) and satellite derived surface CHL (circles) in (a) AEs and (b) CEs. The vertical bars denote the standard deviation of satellite CHL. Note that the model output was forced by climatological mean.

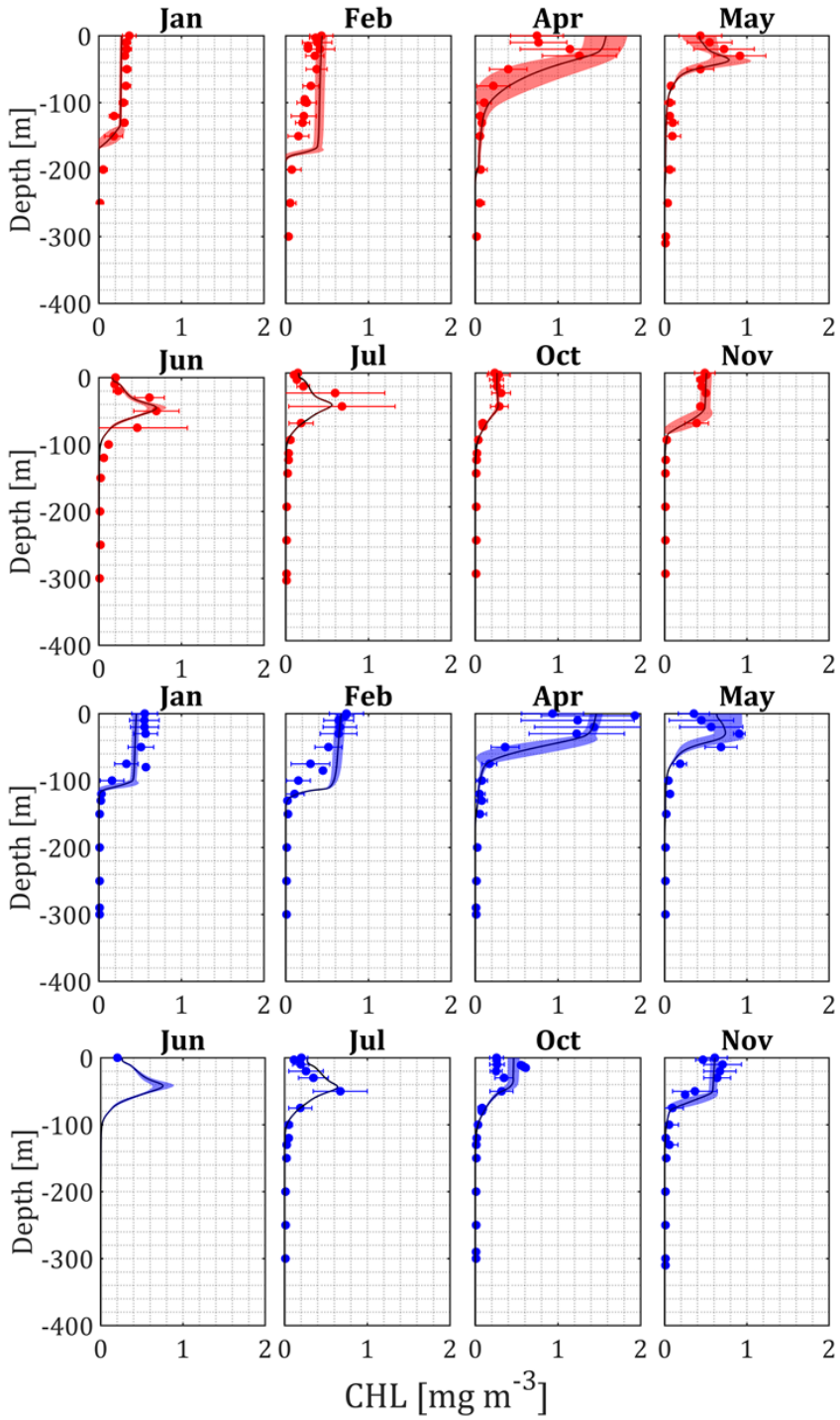

Figure 3.8. Monthly mean vertical distributions of simulated (lines) and observed (filled circles) CHL in AEs (red) and CEs (blue). Horizontal bars indicate the standard deviation of observations. Shading in the lines indicates the standard deviation of the simulated monthly mean. Omitted months correspond to those with no observations.

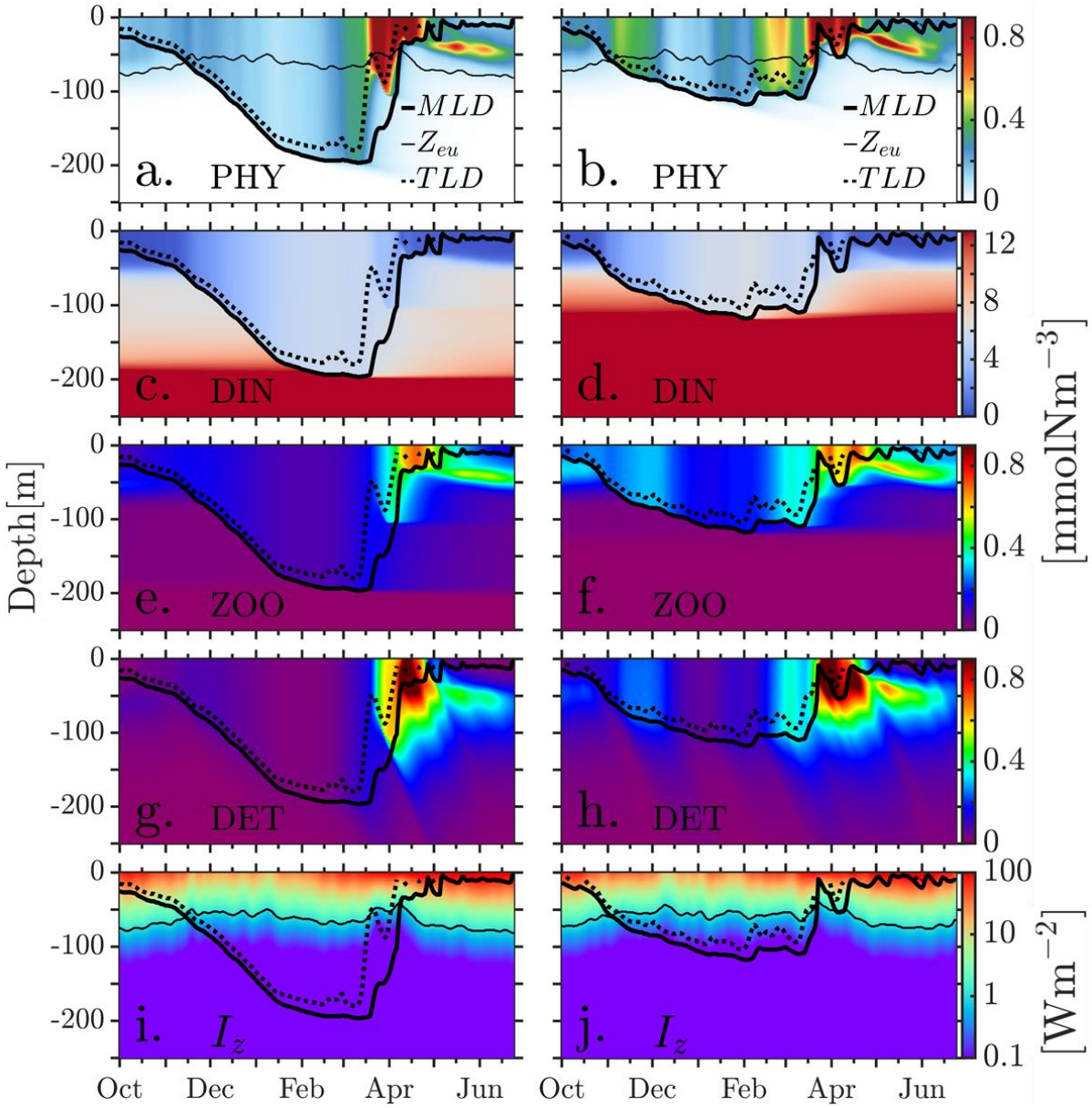

Figure 3.9. Vertical distributions of daily averaged (a-b) PHY, (c-d) DIN, (e-f) ZOO, (g-h) DET (all in mmolN m^{-3}) and (i-j) I_z (in W m^{-2}) in A249 (a, c, e, g, and i) and C325 (b, d, f, h, and j). Thick, thin and doted lines denote MLD, Z_{eu}, and TLD, respectively. For easy comparison the x-axis in A249 and C325 were plot within a similar time period (from October to June).

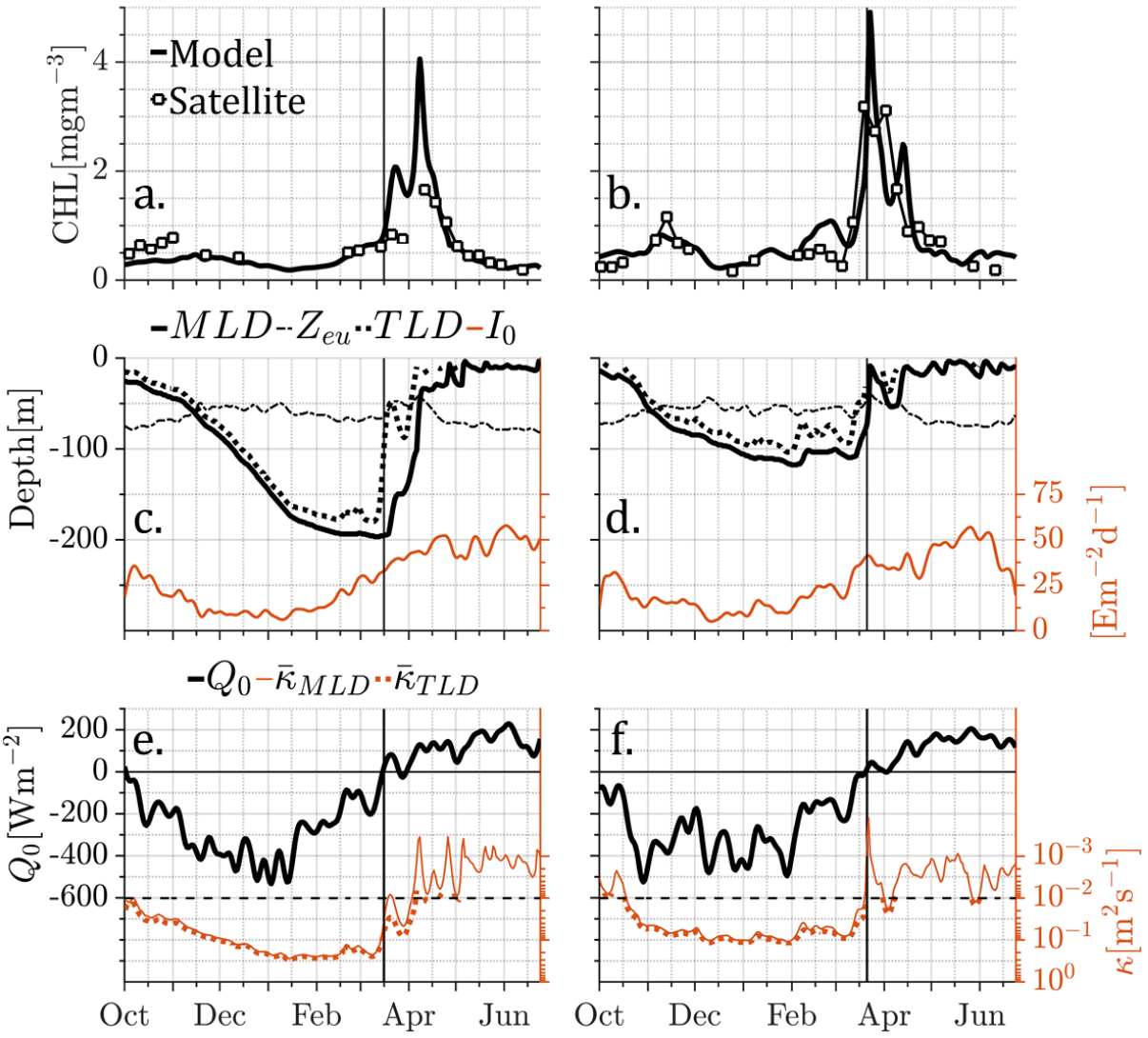

Figure 3.10. Time series of (a-b) surface CHL (model: thick lines, satellite: markers), (c-d) MLD, Z_{eu}, and TLD (thick solid, thin dash-dot, thick dotted lines, respectively, left axis), and I_0 (solid lines, right axis), (e-f) Q_0 (thick solid lines, left axis), and κ averaged over MLD ($\bar{\kappa}_{MLD}$) and over TLD ($\bar{\kappa}_{TLD}$) (thin solid and thick dotted lines, right axis) in A249 (a, c, and e) and C325 (b, d, and f). Vertical solid lines show the shutdown convection time when Q_0 turns positive. Horizontal dashed lines (e-f) indicate reference lines for κ (10^{-2} m^2 s^{-1}). Note that κ (e-f, right axis) increases downward.

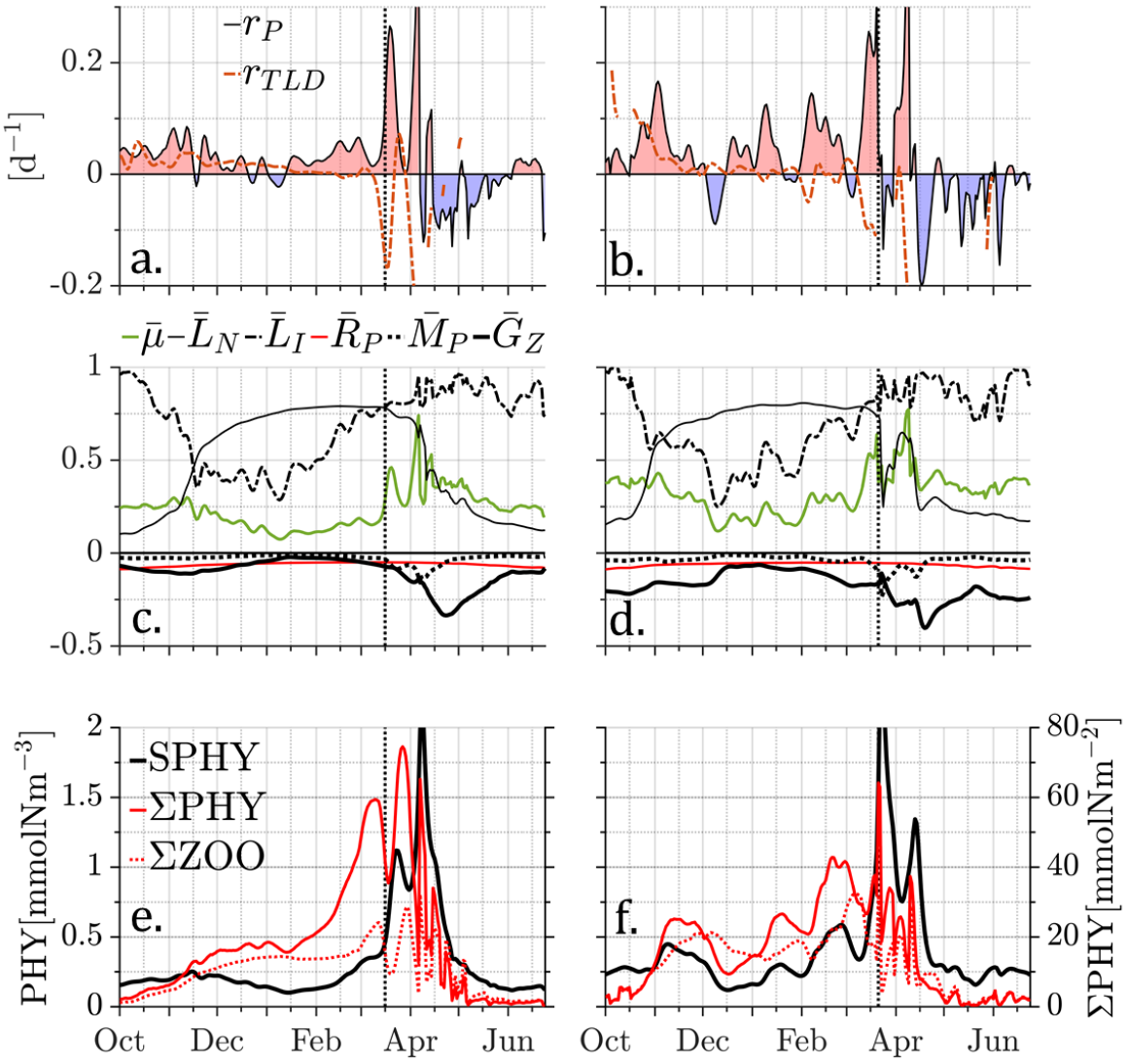

Figure 3.11. Time series of rates controlling PHY biomass and of PHY and ZOO surface and integrated concentrations in A249 (a, c and e) and in C325 (b, d and f) from October to June. (a-b) $\boldsymbol{r_P}$ (solid lines and shades, red (positive) and blue (negative)) and $\boldsymbol{r_{TLD}}$ (dash-dot lines). (c-d) integrated rates of PHY division ($\bar{\boldsymbol{\mu}}$, solid green lines), of $\bar{\boldsymbol{L}}_N$ and $\bar{\boldsymbol{L}}_I$ (thin black and dash-dot lines), of respiration ($\bar{\boldsymbol{R}}_{\boldsymbol{P}}$, solid red lines), of mortality ($\bar{\boldsymbol{M}}_{\boldsymbol{P}}$, dotted lines), and of grazing ($\bar{\boldsymbol{G}}_{\boldsymbol{Z}}$, thick black lines). (e-f) surface (SPHY) and integrated PHY and ZOO (thick

lines: left-axis and thin solid and dotted lines: right-axis, respectively). Vertical cyan lines show the shutdown convection time.

Chapter 4

4. General Discussion

Understanding the processes regulating phytoplankton blooms is important not only for understanding the factors regulating primary production but also for the influence on the climate. Marine phytoplankton is thought to contribute a large fraction of the CO_2 sequestration in the atmosphere (Falkowski et al. 1997). The spring bloom, a large increase in phytoplankton concentration, occurs on regular basis in temperate regions. The initiation mechanism is thought to be controlled by physical factors regulating the dynamics on the oceans (Sverdrup, 1953). Particularly, stratification of the upper ocean in spring caused by solar heating results in alleviation of light limitation for phytoplankton trapped in the newly formed seasonal thermocline and triggers a bloom. This mechanism has been the basis for our understanding of the spring phytoplankton bloom initiation in temperate oceans.

Therefore, in Chapter 2 the spring bloom initiation was investigated to understand the possible roles played by mesoscale eddies on spring bloom initiation in temperate oceans. Mesoscale eddies are known to modulate the dynamics of the mixed layer, and thus have the potential to influence the spring bloom dynamics. Our investigation revealed that two distinct processes are observed in eddies depending on whether eddies are anticyclonic or cyclonic. We found, in part, support to the classical Sverdrup hypothesis in that the blooms observed in mesoscale CEs and AEs were largely controlled by the physical dynamics associated with

eddy perturbation of mixed layer depth. However, the conditions for the initiation of the blooms deviate from the classical hypothesis. Thus, we showed that blooms are earlier in the shallow mixed-layer CEs and the conditions for bloom onset are increased light condition within the mixed-layer (Platt et al. 2010; Zhai et al. 2011). More importantly, bloom initiation was observed before the stratification of water column. In the case of deep mixed-layer AEs, we found support to the observations of Townsend et al., (1992) who observed blooms initiated in the absence of stratification. In fact, blooms in AEs were initiated later and the condition for the initiation was the weakening of turbulent mixing at the end of winter cooling when surface heat flux turns into heating. So, the deep mixed-layers observed in the interior of AEs promote deep excursions of phytoplankton during deep winter convective mixing. This, combined with the low light conditions, phytoplankton growth becomes light limited in the interior of AEs. In spring, when net cooling subsides, blooms are triggered due to the decrease in the depth of turbulent mixing while mixed-layer is still deep (Huisman et al. 1999; Taylor and Ferrari 2011; Ferrari et al. 2015). These results suggest that CEs may be regions of continued production from winter through spring whereas AEs may be related with pulsed production observed in spring when improved condition for phytoplankton growth promote the large blooms observed in the surface in April.

In Chapter 3, motivated by results of the previous chapter, we developed a coupled physical-biological model that resolves the temporal and vertical variation of turbulence and verified the results obtained in Chapter 2. Based on the coupled model, the results supported

the hypothesis that mixed-layer depth in eddies makes the difference in the dynamics for the spring bloom initiation (Maúre et al. 2017). The initiation mechanism and the dynamics of the spring phytoplankton blooms differed in AEs and CEs. In with deep mixed-layer AEs, the bloom initiation is delayed until the relaxation of turbulent convective mixing. Conversely, in the shallow mixed-layer CEs, blooms initiate before the end of convective mixing due to early improvement in light conditions with increase in the solar radiation.

In recent years, the role of grazers on bloom initiation has been invoked (Behrenfeld, 2010). In this paradigm, deep turbulent mixing entrains low phytoplankton water from below the mixed layer and dilutes the prey and predator thereby decreasing the grazing pressure. This is thought to largely impact phytoplankton losses than growth, and thus creating conditions for positive net population accumulation (r_P) in mid-winter while mixed layer is deepening. The biological model used allowed the investigation of the grazing pressure on phytoplankton prior to bloom initiation in both AEs and CEs. The results confirmed the expectation for AEs (with the deep mixed-layers) that relaxation of zooplankton grazing initiates a weak winter phytoplankton accumulation, whereas in the shallow mixed-layer CEs, the winter phytoplankton accumulation was faster. As a result, in spring, phytoplankton increased and peaked faster in CEs than in AEs.

In the study area, the initiation timing of the spring phytoplankton blooms has recently been associated with recruitment success of Japanese sardine (Kodama et al. 2018). Later

blooms were found to favour the recruitment success. This means that AEs have the potential of contributing to recruitment success of the Japanese sardine. In other oceanic regions, earlier blooms, as in CEs, are found to enhance the larval survival of haddock (Platt et al. 2003). This means that difference in the timing of the spring blooms between AEs and CEs contributes to recruitment success of different species. That is, in the Japan Sea, for example, where eddies are generally close to each other there is a potential that the integrated blooming in AEs and CEs provides favourable conditions for more species. In the case of the global ocean where eddies can be found either connected or isolated, the above differences in the blooming between AEs and CEs may provide different fish habitats. For example, Logerwell and Smith (2001) found high larval growth and survival of Pacific sardine in the region of the California Current in offshore eddies. The reason was that, these eddies (both cyclonic and anticyclonic) provided good localised growth conditions for primary and secondary production. Thus, the differences in the timing of bloom initiation in eddies have an important role in growth and survival of different fish species.

Chapter 5

5. General Conclusions

5.1. Concluding Remarks

The influence of mesoscale eddies on phytoplankton spring blooms was investigated based on satellite ocean colour imagery, *in situ* observations and model simulation. The Japan Sea was considered as a study area given that mesoscale eddy activity is ubiquitous and intense, and that phytoplankton seasonality has also a remarkable regularity. Moreover, the Japan Sea has been named “ocean in miniature” because it has most of the global ocean features, such as eddies and western boundary currents. Therefore, it provides a good opportunity, not only for the investigation of interlinks between bloom initiation and mesoscale eddy activity, but also for understanding the potential impacts of climate change on the dynamics of the oceans and thus on phytoplankton seasonality, ecosystems dynamics and fisheries in the global ocean.

In this study, the relationship between spring phytoplankton blooms and mesoscale eddies was established. The spring bloom initiation in eddies deviates from the classical mechanism based on the Sverdrup. AEs have a character of a typical high latitude ocean in which deep winter mixing develops during net cooling. However, in spring when net cooling subsides, the initiation of the spring bloom is triggered by the decrease in the depth of turbulent mixing. This allows phytoplankton growth conditions to be enhanced causing a

bloom to occur. In the case of CEs, on account of their shallow mixed layer depths, bloom initiation appears to be controlled increasing surface light which triggers the initiation of bloom prior to the end of net cooling.

This study provides the first insight into the different mechanisms controlling the spring bloom initiation in temperate seas as influenced by mesoscale eddies. While attempts to creating unifying mechanisms of spring bloom initiation have been made (e.g., Chiswell, 2011), they have not included the role of mesoscale eddies which are ubiquitous throughout the global ocean. Therefore, this study suggested that for unifying mechanism of global cycle of phytoplankton spring blooms in temperate regions, the influence of mesoscale eddies should be considered.

5.2. Suggestions for Prospective Research

In this study we clearly demonstrated the role of turbulent convective mixing on phytoplankton bloom initiation in mesoscale eddies. Recent literature has been suggesting that decrease in grazing during winter deep mixing may cause a bloom to initiate while growth conditions for phytoplankton are deteriorating. This is because the impact of the mixed layer deepening is thought to largely impact losses than growth. While we found support for this hypothesis in AEs, further study is needed to clarify the detailed mechanism in eddies.

Ashjian et al. (2005) found large zooplankton in the sourthern part of the Japan Sea. Larger zooplankton are expected in the colder northern waters, north of the subpolar front. Those found south had greater growth in response to more favourable food conditions. The model simulations indicated higher concentrations of zooplankton in CEs. However, it is not clear whether the favourable food conditions were associated with CEs or not.

Another important aspect that needs further consideration is the inter-annual variation of spring phytoplankton blooms in relation to eddy activity. Climate forcing on different time scales may induce different responses on lower trophic levels and ecosystem functioning. For example, mixed layers are suggested to shallow in years with strong El-Ñino Southern Oscillation. However, it is unclear how this mechanism operates in mesoscale eddies. This has the potential of linking mesoscale eddies, spring blooms and fish recruitment success known to have a connection with bloom initiation timing.

References

Barnier, B., Siefridt, L., Marchesiello, P. (1995). Thermal forcing for a global ocean circulation model using a three-year climatology of ECMWF analyses. *Journal of Marine Systems, 6*(4), 363–380. doi:10.1016/0924-7963(94)00034-9

Behrenfeld, M. J. (2010). Abandoning Sverdrup's critical depth hypothesis on phytoplankton blooms. *Ecology, 91*(4), 977–989. doi:10.1890/09-1207.1

Behrenfeld, M. J., Boss, E., Siegel, D. A., & Shea, D. M. (2005). Carbon-based ocean productivity and phytoplanktonphysiology from space. *Global Biogeochemical Cycles, 19*, GB1006. doi:10.1029/2004GB002299

Behrenfeld, M. J., & Boss, E. S. (2006). Beam attenuation and chlorophyll concentration as alternative optical indices of phytoplankton biomass. *Journal of Marine Research, 64*(3), 431–451. doi:10.1357/002224006778189563

Behrenfeld, M. J., & Boss, E. S. (2014). Resurrecting the ecological underpinnings of ocean plankton blooms. *Annual Review of Marine Science, 6*(1), 167–194. doi:10.1146/annurev-marine-052913-021325

Behrenfeld, M. J., Doney, S. C., Lima, I., Boss, E. S., & Siegel, D. A. (2013a). Annual cycles of ecological disturbance and recovery underlying the subarctic Atlantic spring plankton bloom. *Global Biogeochemical Cycles, 27*, 526–540. doi:10.1002/gbc.20050

Behrenfeld, M. J., Doney, S. C., Lima, I., Boss, E. S., & Siegel, D. A. (2013b). Reply to a comment by Stephen M. Chiswell on: "Annual cycles of ecological disturbance and recovery underlying the subarctic Atlantic spring plankton bloom" by M. J. Behrenfeld et al. (2013). *Global Biogeochemical Cycles, 27*, 1294–1296. doi:10.1002/2013GB004720

Bibby, T. S., Gorbunov, M. Y., Wyman, K. W., & Falkowski, P. G. (2008). Photosynthetic community responses to upwelling in mesoscale eddies in the subtropical North Atlantic and Pacific Oceans. *Deep-Sea Research Part II: Topical Studies in Oceanography*, *55*(10-13), 1310–1320. doi:10.1016/j.dsr2.2008.01.014

Boss, E., and M. Behrenfeld (2010). In situ evaluation of the initiation of the North Atlantic phytoplankton bloom. *Geophysical Research Letters, 37*. doi:10.1029/2010GL044174

Brainerd, K., & Gregg, M. (1995). Surface mixed and mixing layer depths. *Deep Sea Research Part I: Oceanographic Research Papers, 42*(9), 1521–1543. doi:10.1016/0967-0637(95)00068-H

Brody, S. R., & Lozier, M. S. (2014). Changes in dominant mixing length scales as a driver of subpolar phytoplankton bloom initiation in the North Atlantic. *Geophysical Research Letters, 41*, 3197–3203. doi:10.1002/2014GL059707

Brody, S. R., Lozier, M. S., & Dunne, J. P. (2013). A comparison ofmethods to determine phytoplankton bloom initiation. *Journal of Geophysical Research, Oceans*, *118*, 2345–2357. doi:10.1002/jgrc.20167

Chelton, D., Schlax, M., & Samelson, R. (2011). Global observations of nonlinear mesoscale eddies. *Progress in Oceanography*, *91*(2), 167–216. doi:10.1016/j.pocean.2011.01.002

Chiswell, S. M. (2011). Annual cycles and spring blooms in phytoplankton: Don't abandon Sverdrup completely. *Marine Ecology Progress Series, 443*. doi:10.3354/meps09453

Chiswell, S. M. (2013). Comment on "Annual cycles of ecological disturbance and recovery underlying the subarctic Atlantic spring plankton bloom". *Global Biogeochemical Cycles, 27*, 1291–1293. doi:10.1002/2013GB004681

Chiswell, S. M., Bradford-Grieve, J., Hadfield, M. G., & Kennan, S. C. (2013). Climatology of surface chlorophyll a, autumn-winter and spring blooms in the southwest Pacific Ocean. *Journal of Geophysical Research: Oceans, 118*, 1003–1018. doi:10.1002/jgrc.20088

Chiswell, S. M., Calil, P., & Boyd, P. (2015). Spring blooms and annual cycles of phytoplankton: A unified perspective. *Journal of Plankton Research, 37*(3), 500–508. doi:10.1093/plankt/fbv021

Cole, H., Henson, S., Martin, A., & Yool, A. (2012). Mind the gap: The impact of missing data on the calculation of phytoplankton phenology metrics. *Journal of Geophysical Research, 117*, C08030. doi:10.1029/2012JC008249

Cole, H., Henson, S., Martin, A., & Yool, A. (2015). Basin-wide mechanisms for spring bloom initiation: How typical is the North Atlantic? *ICES Journal of Marine Science, 72*(6), 2029–2040. doi:10.1093/icesjms/fsu239

Crawford, W. R., Brickley, P. J., Peterson, T. D., & Thomas, A. C. (2005). Impact of Haida eddies on chlorophyll distribution in the eastern Gulf of Alaska. *Deep-Sea Research Part II: Topical Studies in Oceanography, 52*(7-8), 975–989. doi:10.1016/j.dsr2.2005.02.011

Dong, C., McWilliams, J. C., Liu, Y., and Chen, D. (2014). Global heat and salt transports by eddy movement. *Nature Communications, 5*:3294. http://dx.doi.org/10.1038/ncomms4294

Dufois, F., Hardman-Mountford, N., Greenwood, J., Richardson, A., Feng, M., & Matear, R. (2016). Anticyclonic eddies are more productive than cyclonic eddies in subtropical gyres because of winter mixing. *Science Advances, 2*(5), e1600282. doi:10.1126/sciadv.1600282

Dufois, F., Hardman-Mountford, N. J., Greenwood, J., Richardson, A. J., Feng, M., Herbette, S., & Matear, R. (2014). Impact of eddies on surface chlorophyll in the South Indian Ocean. *Journal of Geophysical Research: Oceans, 119*, 8061–8077. doi:10.1002/2014JC010164

Falkowski, P., Ziemann, D., Kolber, Z., & Bienfang, P. (1991). Role of eddy pumping in enhancing primary production in the ocean. *Nature*, *352*(6330), 55–58. doi:10.1038/352055a0

Ferrari, R., Merrifield, S., & Taylor, J. (2015). Shutdown of convection triggers increase of surface chlorophyll. *Journal of Marine Systems*, *147*, 116–122. doi:10.1016/j.jmarsys.2014.02.009

Ferreira, S., Visser, A., MacKenzie, B., & Payne, M. (2014). Accuracy and precision in the calculation of phenology metrics. *Journal of Geophysical Research: Oceans*, *119*, 8438–8453. doi:10.1002/2014JC010323

Fischer, A. D., Moberg, E. A., Alexander, H., Brownlee, E. F., Hunter-Cevera, K. R., Pitz, K. J., Rosengard, S. Z., Sosik, H. M. (2014). Sixty years of Sverdrup: A retrospective of progress in the study of phytoplankton blooms. *Oceanography 27*(1), 222–235. doi:10.5670/oceanog.2014.26

Furuichi, N., Hibiya, T., and Niwa, Y. (2012). Assessment of turbulence closure models for resonant inertial response in the oceanic mixed layer using a large eddy simulation model. *Journal of Oceanography, 68*, 285–294. doi:10.1007/s10872-011-0095-3

Garçon, V. C., Oschlies, A., Doney, S. C., McGillicuddy, D., and Waniek, J. (2001). The role of mesoscale variability on plankton dynamics in the North Atlantic. *Deep Sea Research Part II: Topical Studies in Oceanography, 48*, 2199–2226, doi:10.1016/s0967-0645(00)00183-1

Gaube, P., Chelton, D. B., Strutton, P. G., & Behrenfeld, M. J. (2013). Satellite observations of chlorophyll, phytoplankton biomass, and Ekman pumping in nonlinear mesoscale eddies. *Journal of Geophysical Research: Oceans, 118*, 6349–6370. doi:10.1002/2013JC009027

Gower, J., Denman, K. L., & Holyer, R. J. (1980). Phytoplankton patchiness indicates the fluctuation spectrum of mesoscale oceanic structure. *Nature, 288*, 157–159. doi:10.1038/288157a0

Hitchcock, G. L., and Smayda, T. J. (1977). The importance of light in the initiation of the 1972-1973 winter-spring diatom bloom in Narragansett Bay. *Limnology and Oceanography, 22*, 126–131. doi:10.4319/lo.1977.22.1.0126

Holte, J., & Talley, L. (2009). A new algorithm for finding mixed layer depths with applications to argo data and subantarctic mode water formation. Journal of *Atmospheric and Oceanic Technology, 26*(9), 1920–1939. doi:10.1175/2009JTECHO543.1

Huisman, J., van Oostveen, P., & Weissing, F. (1999). Critical depth and critical turbulence: Two different mechanisms for the development of phytoplankton blooms. *Limnology and Oceanography, 44*(7), 1781–1787. doi:10.4319/lo.1999.44.7.1781

Hunt, G. L., Stabeno, P., Walters, G., Sinclair, E., Brodeur, R., Napp, J., & Bond, N. (2002). Climate change and control of the southeastern Bering Sea pelagic ecosystem. *Deep Sea Research, Part II, 49*(26), 5821–5853. doi:10.1016/S0967-0645(02)00321-1

Isoda, Y. (1994). Warm eddy movements in the eastern Japan Sea. *Journal of Oceanography*, 50(1), 1–15. doi:10.1007/BF02233852

Itoh, S., Yasuda, I., Saito, H., Tsuda, A., and Komatsu, K. (2015). Mixed layer depth and chlorophyll a: Profiling float observations in the Kuroshio–Oyashio Extension region. *Journal of Marine Systems, 151*, 1–14. doi:10.1016/j.jmarsys.2015.06.004

Kahru, M., Brotas, V., Manzano-Sarabia, M., & Mitchell, B. G. (2011). Are phytoplankton blooms occurring earlier in the Arctic? *Global Change Biology, 17*(4), 1733–1739. doi:10.1111/j.1365-2486.2010.02312.x

Kim, H., Yoo, S., & Oh, I. S. (2007). Relationship between phytoplankton bloom and wind stress in the sub-polar frontal area of the Japan/East Sea. *Journal of Marine Systems, 67*(3–4), 205–216. doi:10.1016/j.jmarsys.2006.05.016

Kodama, T., Wagawa, T., Ohshimo, S., Morimoto, H., Iguchi, N., Fukudome, K., Goto, T., Takahashi, M., and Yasuda, Y. (2018) Improvement in recruitment of Japanese sardine with delays of the spring phytoplankton bloom in the Sea of Japan. *Fisheries Oceanography*. 1–13. doi:10.1111/fog.12252

Koeller, P. F.-Y. C., Platt, T., Sathyendranath, S., Richards, A., Oullet, P., Orr, D., & Aschan, M. (2009). Basin-scale coherence in phenology of shrimps and phytoplankton in the North Atlantic Ocean. *Science, 324*(5928), 791–793. doi:10.1126/science.1170987

Kouketsu, S., Tomita, H., Oka, E., Hosoda, S., Kobayashi, T., & Sato, K. (2012). The role ofmeso-scale eddies inmixed layer deepening and mode water formation in the western North Pacific. *Journal of Oceanography, 68*(1), 63–77. doi:10.1007/s10872-011-0049-9

Kuhn A. M., Fennel, K., Mattern, J. P. (2015). Model investigations of the North Atlantic spring bloom initiation. *Progress in Oceanography, 138*, 176–193. doi:10.1016/j.pocean.2015.07.004

Lévy, M. (2015). Exploration of the critical depth hypothesis with a simple NPZ model. *ICES Journal of Marine Science, 72*, 1916–1925. doi:10.1093/icesjms/fsv016

Lim, J.-H., Son, S., Park, J.-W., Kwak, J., Kang, C.-K., Son, Y.,…Lee, S. (2012). Enhanced biological activity by an anticyclonic warm eddy during early spring in the East Sea (Japan Sea) detected by the geostationary ocean color satellite. *Ocean Science Journal, 47*(3), 377–385. doi:10.1007/s12601-012-0035-1

Lim, S., Jang, C., Oh, I., & Park, J. (2012). Climatology of the mixed layer depth in the East/Japan Sea. *Journal of Marine Systems, 96-97*, 1–14. doi:10.1016/j.jmarsys.2012.01.003

Logerwell, E., & Smith, P. (2001). Mesoscale eddies and survival of late stage Pacific sardine (Sardinops sagax) larvae. *Fisheries Oceanography, 10*(1), 13–25. doi:10.1046/j.1365-2419.2001.00152.x

Mahadevan, A., D'Asaro, E., Lee, C., & Perry,M. (2012). Eddy-driven stratification initiates North Atlantic spring phytoplankton blooms. *Science, 337*, 54–58. doi:10.1126/science.1218740

Mann, K. H., & Lazier, J. R. N. (1996). *Dynamics of marine ecosystems: Biological-physical interactions in the oceans* (2nd ed., pp. 56–97). Cambridge, MA: Blackwell Science, Inc.

Marra, J. F., Dickey, T. D., Plueddemann, A. J., Weller, R. A., Kinkade, C. S., Stramska, M. (2015). Phytoplankton bloom phenomena in the North Atlantic Ocean and Arabian Sea. *ICES Journal of Marine Science, 72*, 2021–2028. doi:10.1093/icesjms/fsu241.

Maúre, E. R., Ishizaka, J., Sukigara, C., Mino, Y., Aiki, H., Matsuno, T., Tomita, H., Goes, J. I., and Gomes, H. R. (2017). Mesoscale Eddies Control the Timing of Spring Phytoplankton Blooms: A Case Study in the Japan Sea. *Geophys Research Letters, 44*, 11,115–11,124. doi:10.1002/2017GL074359

McGillicuddy, D. J., and Robinson, A. R. (1997). Eddy-induced nutrient supply and new production in the Sargasso Sea. *Deep Sea Research Part I: Oceanographic Research Papers, 44*, 1427–1450. doi:10.1016/S0967-0637(97)00024-1

McGillicuddy, D. J., Johnson, R., Siegel, D. A., Michaels, A. F., Bates, N. R., and Knap, A. H.(1999). Mesoscale variations of biogeochemical properties in the Sargasso Sea. *Journal of Geophysical Research: Oceans, 104*, 13381–13394. doi:10.1029/1999JC900021

McGillicuddy, D. J., McCarthy, J. J., Robinson, A. R. (1995). Coupled physical and biological modeling of the spring bloom in the North Atlantic (I): model formulation and one dimensional bloom processes. *Deep Sea Research Part I: Oceanographic Research Papers, 42*, 1313-1357. doi:10.1016/0967-0637(95)00034-4

McGillicuddy, D. J. (2016). Mechanisms of physical-biological-biogeochemical interaction at the oceanic mesoscale. *Annual Review of Marine Science, 8*(1), 125–159. doi:10.1146/annurev-marine-010814-015606

McGillicuddy, D. J., Robinson, A. R., Siegel, D. A., Jannasch, H. W., Johnson, R., Dickey, T. D., McNeil, J., Michaels, A. F., and Knap, A. H. (1998) Influence of mesoscale eddies on new production in the Sargasso Sea. *Nature, 394*, 263–266. http://dx.doi.org/10.1038/28367

Mellor, G. L. (2001). One-Dimensional, Ocean Surface Layer Modeling: A Problem and a Solution. *Journal of Physical Oceanography*, 790–809. doi:10.1175/1520-0485(2001)031<0790:ODOSLM>2.0.CO;2

Mellor, G. L., and Yamada, T. (1982). Development of a turbulence closure model for geophysical fluid problems. *Reviews of Geophysics, 20*, 851-875. doi:10.1029/RG020i004p00851

Mignot, A., Ferrari, R., and Claustre, H. (2018). Floats with bio-optical sensors reveal what processes trigger the North Atlantic bloom. *Nature Communications, 9*, 190. doi:10.1038/s41467-017-02143-6

Moisan, J. R., Miller, A. J., Di Lorenzo, E., Wilkin, J. (2005). Modeling and data assimilation. *Remote sensing of coastal aquatic environments technologies, techniques and applications* (Chapter 13, pp. 229–257). Springer

Moisan, J. R., and Hofmann, E. E. (1996). Modeling nutrient and plankton processes in the California coastal transition zone: 1. A time- and depth-dependent model. *Journal of Geophysical Research: Oceans, 101*, 22647–22676. doi:10.1029/96JC01718

Morimoto, A., Yanagi, T., & Kaneko, A. (2000). Eddy field in the Japan Sea derived from satellite altimetric data. *Journal of Oceanography, 56*, 449–462. doi:10.1023/A:1011184523983

Nakanishi, M., and H. Niino, 2009: Development of an Improved Turbulence Closure Model for the Atmospheric Boundary Layer. *Journal of the Meteorological Society of Japan, 87*, 895–912. doi:10.2151/jmsj.87.895

Nencioli, F., Dong, C., Dickey, T., Washburn, L., & McWilliams, J. (2010). A vector geometry–based eddy detection algorithmand its application to a high-resolution numerical model product and high-frequency radar surface velocities in the Southern California Bight. *Journal of Atmospheric and Oceanic Technology, 27*(3), 564–579. doi:10.1175/2009JTECHO725.1

Omand, M. M., D'Asaro E. A., Lee C. M., Perry, M. J., Briggs, N., Cetinić, I., and Mahadevan, A. (2015). Eddy-driven subduction exports particulate organic carbon from the spring bloom. Science, 348, 222–225. doi:10.1126/science.1260062

Onitsuka, G., & Yanagi, T. (2005). Differences in ecosystem dynamics between the northern and southern parts of the Japan Sea: Analyses with two ecosystem models. *Journal of Oceanography*, *61*(3), 415–433. doi:10.1007/s10872-005-0051-1

Paulson, C. A., and Simpson, J. J. (1977). Irradiance measurements in the upper ocean. *Journal of Physical Oceanography, 7*, 952–956. doi:10.1175/1520-0485(1977)007<0952:IMITUO>2.0.CO;2

Platt, T., Fuentes-Yaco, C., & Frank, K. (2003). Marine ecology: Spring algal bloom and larval fish survival. *Nature*, *423*(6938), 398–399. doi:10.1038/423398b

Platt, T., Sathyendranath, S., White, G., Fuentes-Yaco, C., Zhai, L., Devred, E., & Tang, C. (2010). Diagnostic properties of phytoplankton time series from remote sensing. *Estuaries and Coasts, 33*(2), 428–439. doi:10.1007/s12237-009-9161-0

Riley, G. (1946). Factors controlling phytoplankton populations on Georges Bank. *Journal of Marine Research, 6*, 54–73.

Riley, G. (1942). The relationship of vertical turbulence and spring diatom flowering. *Journal of Marine Research, 5*, 67–87.

Scott, V., Kettle, H., and Merchant, C. J. (2011). Sensitivity analysis of an ocean carbon cycle model in the North Atlantic: an investigation of parameters affecting the air-sea CO2 flux, primary production and export of detritus. *Ocean Science, 7,* 405–419. doi:10.5194/os-7-405-2011

Siegel, D. A., Doney, S. C., & Yoder, J. A. (2002). The North Atlantic spring phytoplankton bloom and Sverdrup's critical depth hypothesis. *Science, 296*(5568), 730–733. doi:10.1126/science.1069174

Smetacek, V., and Passow, U. (1990). Spring bloom initiation and Sverdrup's critical-depth model. *Limnology and Oceanography 35*:228–234. doi:10.4319/lo.1990.35.1.0228

Sugimoto, T., & Tameishi, H. (1992). Warm-core rings, streamers and their role on the fishing ground formation around Japan. *Deep Sea Research Part A, 39,* S183–S201. doi:10.1016/S0198-0149(11)80011-7

Sukigara, C., Suga, T., Toyama, K., & Oka, E. (2014). Biogeochemical responses associated with the passage of a cyclonic eddy based on shipboard observations in the western North Pacific. *Journal of Oceanography, 70,* 435–445. doi:10.1007/s10872-014-0244-6

Sverdrup, H. U. (1953). On conditions for the vernal blooming of phytoplankton. ICES *Journal of Marine Science, 18*(3), 287–295. doi:10.1093/icesjms/18.3.287

Sweeney, E., McGillicuddy, D., & Buesseler, K. (2003). Biogeochemical impacts due to mesoscale eddy activity in the Sargasso Sea as measured at the Bermuda Atlantic Time-series Study (BATS). *Deep Sea Research, Part II, 50*(22-26), 3017–3039. doi:10.1016/j.dsr2.2003.07.008

Symonds, M., & Moussalli, A. (2011). A brief guide to model selection, multimodel inference and model averaging in behavioural ecology using Akaike's information criterion. *Behavioral Ecology and Sociobiology, 65*(1), 13–21. doi:10.1007/s00265-010-1037-6

Taylor, J., & Ferrari, R. (2011). Shutdown of turbulent convection as a new criterion for the onset of spring phytoplankton blooms. *Limnology and Oceanography, 56*(6), 2293–2307. doi:10.4319/lo.2011.56.6.2293

Tilburg, C., Subrahmanyam, B., & O'Brien, J. (2002). Ocean color variability in the Tasman Sea. *Geophysical Research Letters, 29*(10), 1487. doi:10.1029/2001GL014071

Townsend, D., Cammen, L., Holligan, P., Campbell, D., & Pettigrew, N. (1994). Causes and consequences of variability in the timing of spring phytoplankton blooms. *Deep Sea Research, Part I, 41*(5-6), 747–765. doi:10.1016/0967-0637(94)90075-2

Townsend, D. W., & Cammen, L. M. (1988). Potential importance of the timing of spring plankton blooms to benthic-pelagic coupling and recruitment of juvenile demersal

fishes. *Biological Oceanography, 5*(3), 215–228. doi:10.1080/01965581.1987.10749514

Venables, H., and Moore, C. M. (2010). Phytoplankton and light limitation in the Southern Ocean: Learning from high-nutrient, high-chlorophyll areas. *Journal of Geophysical Research: Oceans, 115*. doi:10.1029/2009JC005361

Yoshie, N., Yamanaka, Y., Kishi, M. J., and Saito, H. (2003) One Dimensional Ecosystem Model Simulation of the Effects of Vertical Dilution by the Winter Mixing on the Spring Diatom Bloom. *Journal of Oceanography, 59,* 563–571. doi: 10.1023/B:JOCE.0000009586.02554.d3

Wagenmakers, E.-J., & Farrell, S. (2004). AIC model selection using Akaike weights. *Psychonomic Bulletin & Review, 11*(1), 192–196. doi:10.3758/BF03206482

Williams, R. (1988). Modification of ocean eddies by air-sea interaction. *Journal of Geophysical Research: Oceans, 93,* 15,523–15,533. doi:10.1029/JC093iC12p15523

Yamada, K., & Ishizaka, J. (2006). Estimation of interdecadal change of spring bloom timing, in the case of the Japan Sea. *Geophysical Research Letters, 33,* L02608. doi:10.1029/2005GL024792

Yamada, K., Ishizaka, J., Yoo, S., Kim, H., & Chiba, S. (2004). Seasonal and interannual variability of sea surface chlorophyll a concentration in the Japan/East Sea (JES). *Progress in Oceanography, 61*, 193–211. doi:10.1016/j.pocean.2004.06.001

Zhai, L., Platt, T., Tang, C., Sathyendranath, S., & Walls, R. (2011). Phytoplankton phenology on the Scotian Shelf. *ICES Journal of Marine Science, 68*(4), 781–791. doi:10.1093/icesjms/fsq175

Zhang, Z., Wang, W., and Qiu, B. (2014). Oceanic mass transport by mesoscale eddies. *Science, 345*(6194), 322-324. doi: 10.1126/science.1252418